Non-invasive Diagnostic Approaches for Giant Cell Arteritis

Naumovska, Magdalena

2024

Document Version:
Publisher's PDF, also known as Version of record

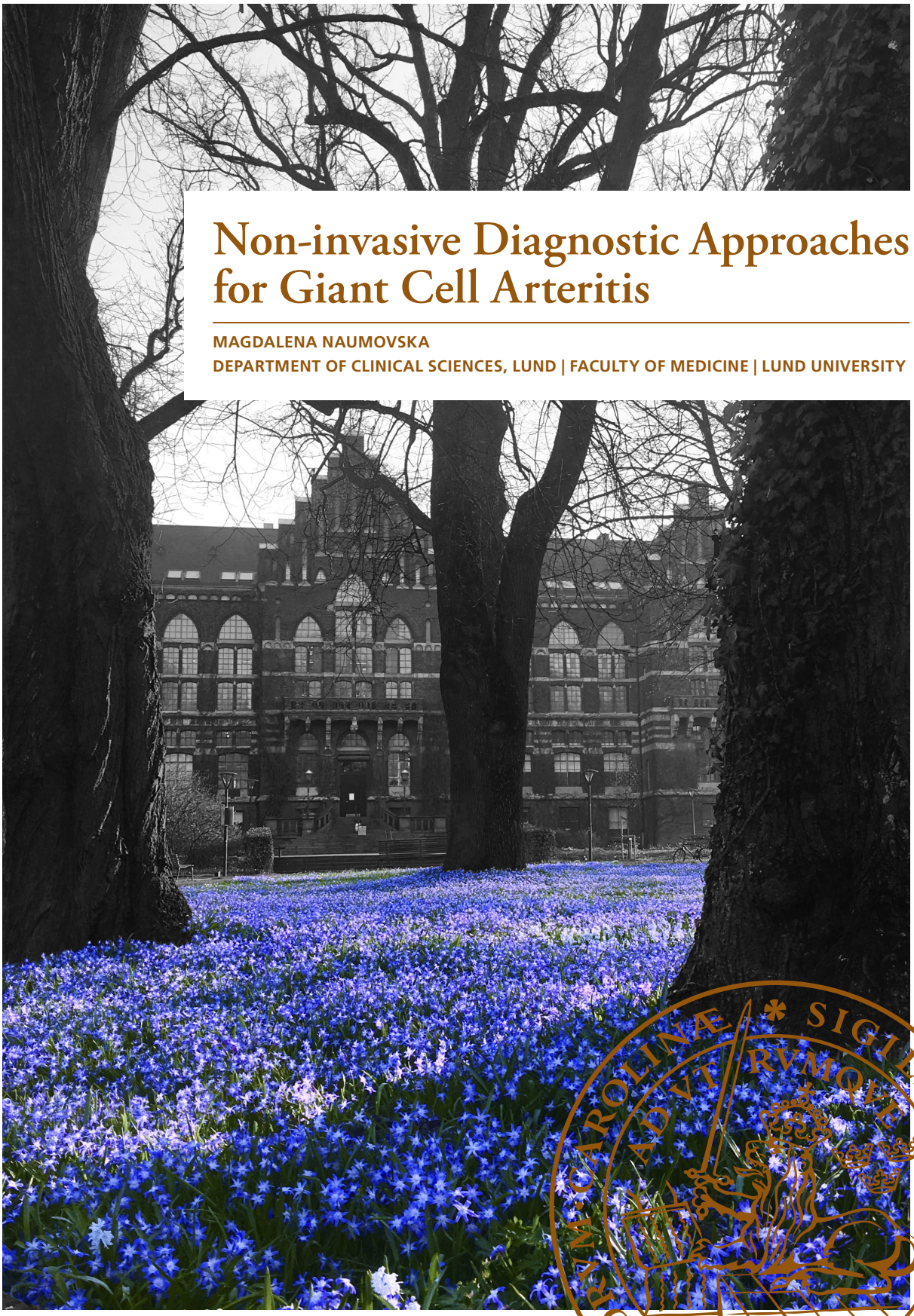

Non-invasive Diagnostic Approaches for Giant Cell Arteritis

MAGDALENA NAUMOVSKA
DEPARTMENT OF CLINICAL SCIENCES, LUND | FACULTY OF MEDICINE | LUND UNIVERSITY

Printed by Media-Tryck, Lund 2024 NORDIC SWAN ECOLABEL 3041 0903

MAGDALENA NAUMOVSKA received her medical degree from Lund University in 2010. She works at Skåne University Hospital as an ophthalmologist specialized in neuroophthalmology. Her main area of research is within the field of neuroophthalmology. This thesis explores novel non-invasive techniques for diagnosing giant cell arteritis.

LUND UNIVERSITY

FACULTY OF MEDICINE

Department of Clinical Sciences, Lund
Ophthalmology

Lund University, Faculty of Medicine
Doctoral Dissertation Series 2024:45
ISBN 978-91-8021-538-1
ISSN 1652-8220

Non-invasive Diagnostic Approaches for Giant Cell Arteritis

Magdalena Naumovska, MD

LUND
UNIVERSITY

DOCTORAL DISSERTATION
by due permission of the Faculty of Medicine, Lund University, Sweden.
To be defended at 13.00 on May 2nd 2024, in LUX Aula, Helgonavägen 3, Lund, Sweden

Faculty opponent
Gauti Jóhannesson, MD, PhD
Associate professor, Umeå University, Umeå, Sweden

Document name: DOCTORAL DISSERTATION

Organization: LUND UNIVERSITY
Faculty of Medicine
Department of Clinical Sciences Lund, Ophthalmology, Lund Sweden

Date of issue: 2024-04-11

Sponsoring organization:

Author(s): Magdalena Naumovska

Title and subtitle: Non-invasive Diagnostic Approaches for Giant Cell Arteritis

Abstract:

Giant cell arteritis (GCA) is a treatable, but potentially sight-threatening form of primary systemic vasculitis. Prompt and correct diagnosis is important, as early intervention can prevent blindness and other serious vascular events. Diagnosing GCA presents a clinical challenge as there are no diagnostic criteria for the disease, and the symptoms are often initially diffuse. Temporal artery biopsy (TAB) has long been regarded as the gold standard for diagnosing GCA, but has low diagnostic sensitivity and is associated with surgical risks. A non-invasive diagnostic method would therefore be of great benefit. Previous attempts, employing methods like ultrasound, have shown variable accuracy in diagnostic performance.

The aim of the work presented in this thesis was to assess three novel non-invasive techniques for future GCA diagnosis: photoacoustic imaging (PAI), ultrasound center frequency shift (CFS), and tomographic three-dimensional (3D) ultrasound.

PAI is a biomedical technique that uses the combination of laser light and ultrasound and provides high-resolution images of biological tissues. The technique was evaluated with regard to its safety and patient tolerability, and the spectral signature of the temporal artery in healthy subjects was obtained. PAI was well tolerated by the participants and did not affect their visual function. The spectral signature of the temporal artery was unique, and the artery could be clearly differentiated from the surrounding tissue. PAI was also evaluated with respect to spectral and spatial characterization of the temporal artery *ex vivo* from subjects suspected of having GCA. PAI provided detailed spectral information allowing the architecture of the temporal artery to be mapped. Spectral analysis indicated a difference in the spectra obtained from GCA-positive and GCA-negative biopsies.

Ultrasound CFS, a novel ultrasound technique that provides objective information on tissue microstructure, was assessed on TAB specimens from subjects suspected of having GCA. The mean CFS, expressed as CFS (%), decreased significantly less in vessels with GCA than in vessels without GCA, indicating that ultrasound CFS has the potential to discriminate between GCA-positive and GCA-negative biopsies.

Tomographic 3D ultrasound was used to visualize the temporal artery in healthy subjects and in patients with suspected GCA. The inner and outer vessel diameters were measured, and the vessel wall fraction was calculated. This technique enabled 3D visualization of the temporal artery, and the high vessel wall fraction revealed vessel wall thickening and lumen narrowing, which may be indicative of GCA.

Histopathological examinations of TAB specimens were used as references for diagnosing GCA in the studies presented in this thesis, and since the diagnostic sensitivity of TAB may vary with biopsy length, it was investigated whether the length of the TAB specimen decreased after excision and formalin fixation, as indicated in previous studies. The length of the biopsy was measured before excision, after excision, and after formalin fixation. The median length decreased following excision, but no further reduction was seen as a result of formalin fixation. The surgeon can therefore be confident that the length of the biopsy after excision is the length examined histopathologically.

In conclusion, PAI, ultrasound CFS, and tomographic 3D ultrasound are promising non-invasive diagnostic tools for GCA. Further technical development and studies are needed before their clinical applicability can be assessed.

Key words: Giant cell arteritis, temporal arteritis, photoacoustic imaging, ultrasound, non-invasive diagnostics

Classification system and/or index terms (if any)

Supplementary bibliographical information

Language: English

ISSN and key title: 1652-8220

ISBN: 978-91-8021-538-1

Recipient's notes

Number of pages:74

Price

Security classification

Non-invasive Diagnostic Approaches for Giant Cell Arteritis

Magdalena Naumovska, MD

LUND
UNIVERSITY

Lund University, Faculty of Medicine, Doctoral Dissertation Series 2024:45

ISBN 978-91-8021-538-1

ISSN 1652-8220

Printed in Sweden by Media-Tryck, Lund University, Lund 2024

To my mother and father

“Per aspera ad astra”

Contents

Abstract

Giant cell arteritis (GCA) is a treatable, but potentially sight-threatening form of primary systemic vasculitis. Prompt and correct diagnosis is important, as early intervention can prevent blindness and other serious vascular events. Diagnosing GCA presents a clinical challenge as there are no diagnostic criteria for the disease, and the symptoms are often initially diffuse. Temporal artery biopsy (TAB) has long been regarded as the gold standard for diagnosing GCA, but has low diagnostic sensitivity and is associated with surgical risks. A non-invasive diagnostic method would therefore be of great benefit. Previous attempts, employing methods like ultrasound, have shown variable accuracy in diagnostic performance.

The aim of the work presented in this thesis was to assess three novel non-invasive techniques for future GCA diagnosis: photoacoustic imaging (PAI), ultrasound center frequency shift (CFS), and tomographic three-dimensional (3D) ultrasound.

PAI is a biomedical technique that uses the combination of laser light and ultrasound and provides high-resolution images of biological tissues. The technique was evaluated with regard to its safety and patient tolerability, and the spectral signature of the temporal artery in healthy subjects was obtained. PAI was well tolerated by the participants and did not affect their visual function. The spectral signature of the temporal artery was unique, and the artery could be clearly differentiated from the surrounding tissue. PAI was also evaluated with respect to spectral and spatial characterization of the temporal artery *ex vivo* from subjects suspected of having GCA. PAI provided detailed spectral information allowing the architecture of the temporal artery to be mapped. Spectral analysis indicated a difference in the spectra obtained from GCA-positive and GCA-negative biopsies.

Ultrasound CFS, a novel ultrasound technique that provides objective information on tissue microstructure, was assessed on TAB specimens from subjects suspected of having GCA. The mean CFS, expressed as CFS (%), decreased significantly less in vessels with GCA than in vessels without GCA, indicating that ultrasound CFS has the potential to discriminate between GCA-positive and GCA-negative biopsies.

Tomographic 3D ultrasound was used to visualize the temporal artery in healthy subjects and in patients with suspected GCA. The inner and outer vessel diameters were measured, and the vessel wall fraction was calculated. This technique enabled 3D visualization of the temporal artery, and the high vessel wall fraction revealed vessel wall thickening and lumen narrowing, which may be indicative of GCA.

Histopathological examinations of TAB specimens were used as references for diagnosing GCA in the studies presented in this thesis, and since the diagnostic sensitivity of TAB may vary with biopsy length, it was investigated whether the length of the TAB specimen decreased after excision and formalin fixation, as indicated in previous studies. The length of the biopsy was measured before excision, after excision, and after formalin fixation. The median length decreased following excision, but no further reduction was seen as a result of formalin fixation. The surgeon can therefore be

confident that the length of the biopsy after excision is the length examined histopathologically.

In conclusion, PAI, ultrasound CFS, and tomographic 3D ultrasound are promising non-invasive diagnostic tools for GCA. Further technical development and studies are needed before their clinical applicability can be assessed.

Populärvetenskaplig sammanfattning

Jättecellsarterit (*giant cell arteritis*, GCA), även kallad temporalisarterit, är en inflammatorisk kärlsjukdom som nästan uteslutande drabbar personer över 50 år. Orsaken till inflammationen i kärlen är okänd och sjukdomen är ovanlig (cirka 13 fall/100 000 invånare och år i Skåne hos individer över 50 år), men den är vanligare i Skandinavien jämfört med i övriga länder. Trots detta misstänks sjukdomen ofta inom sjukvården runt om i landet. Detta beror på den medvetenhet som finns om de förödande konsekvenserna som en missad diagnos kan medföra. Obehandlad jättecellsarterit kan leda till syrebrist (infarkt) i synnerven eller i hjärnan, med blindhet eller stroke som följd. För att förhindra kärlkomplikationer, i synnerhet blindhet, är det därför av yttersta vikt att behandlingen inte fördröjs. Jättecellsarterit behandlas med höga doser kortison, vilket vanligtvis ges under lång tid. Behandlingen är dock förknippad med biverkningar och för att undvika att friska personer behandlas i onödan är det därför viktigt med en korrekt ställd diagnos. Jättecellsarterit kan emellertid vara en utmanande diagnos att fastställa eftersom det inte finns något specifikt blodprov eller diagnoskriterier för sjukdomen. Dessutom varierar symptomen beroende på vilka kärl som är drabbade och symptomen är ofta initialt diffusa, såsom trötthet, sjukdomskänsla, feber och viktnedgång. Vissa har mer typiska symptom som huvudvärk, tuggsmärtor och ömhet i hårbotten, men inte heller dessa symptom är specifika för sjukdomen.

Diagnosen ställs idag genom att det tas ett vävnadsprov (biopsi) av ett kärl i tinningen, som därefter analyseras i mikroskop för att identifiera inflammation i kärlet. Ingreppet är inte helt riskfritt och kan i vissa fall leda till infektion, blödning eller nervskador. Hos 15-30% med jättecellsarterit är provsvaret dessutom felaktigt normalt, vilket exempelvis kan bero på långvarig kortisonbehandling innan biopsin, att för kort biopsi tas eller att inflammationen i kärlet ibland förekommer fläckvis. Metoden anses därför vara osäker. Tidigare försök att använda en icke-invasiv diagnostisk metod, främst ultraljud och magnetkameraundersökning (MR), har visat otillfredsställande resultat av flera anledningar, såsom låg diagnostisk träffsäkerhet, låg tillgänglighet, att tekniken är dyr eller att den är beroende av undersökarens skicklighet. Det finns således idag ingen icke-invasiv metod för att ställa diagnosen jättecellsarterit som med säkerhet helt kan ersätta kirurgisk biopsi av tinningkärlet.

På senare år har flera nya metoder utvecklats för att avbilda vävnader och kärl med goda resultat. I denna avhandling undersöks tre nya tekniker för att i framtiden diagnostisera jättecellsarterit: fotoakustisk avbildning (*photoacoustic imaging*, förkortat PAI), högfrekvent ultraljud med analys av skiftet i central frekvens (*center frequency shift,* förkortat CFS) och tomografiskt tredimensionellt (3D) ultraljud.

I Studie I testades PAI på tinningkärlet hos friska individer. PAI har tidigare visats ge en tydlig bild av vävnaders struktur utifrån dess molekylära sammansättning genom att kombinera laserljus och ultraljud. Vid PAI belyses vävnaden med laserljus i korta pulsar, vilket ger en mycket liten temperaturökning och en rörelse i vävnadens små byggstenar (molekyler), som börjar dansa i takt med ljuset. Detta skapar små ljudvågor, som fångas upp av en ultraljudsmottagare och informationen bearbetas sedan till en

detaljrik 3D-bild. Syftet med Studie I var att undersöka hur tinningkärlet ser ut med PAI (dess ”optiska fingeravtryck”) hos friska individer och att bekräfta metodens säkerhet ur ögonsynpunkt. PAI bedömdes vara säkert vad gäller synfunktioner och undersökningen tolererades väl. Tinningkärlets optiska fingeravtryck var specifikt och kärlet kunde tydligt urskiljas från omgivande vävnad.

I Studie II undersöktes PAI på biopsier av tinningkärlet hos individer med misstänkt jättecellsarterit. Med PAI kunde kärlets arkitektur tydligt kartläggas och ge detaljrika bilder av kärlväggen. Efter bearbetning och analys av data fanns det en antydan till att den spektrala signaturen, som reflekterar den molekylära sammansättningen, skiljer sig mellan biopsier som är positiva för jättecellsarterit jämfört med de som är negativa för jättecellsarterit.

I Studie III testades högfrekvent ultraljud med analys av skiftet i central frekvens (ultraljud CFS) på biopsier av tinningkärlet hos personer med misstänkt jättecellsarterit. Ultraljud CFS har tidigare visats kunna identifiera komponenter i kärlförkalkningar som associeras med risken för kärlkomplikationer, såsom stroke. Ultraljud CFS ger ett objektivt mått och är inte lika beroende av undersökarens skicklighet, vilket annars begränsar bedömningen av en ultraljudsundersökning. Resultaten visade att CFS-värdet i procent minskade mindre hos de som hade en positiv biopsi för jättecellsarterit jämfört med de som hade en negativ biopsi, vilket indikerar att ultraljud CFS har potential att skilja kärlbiopsier med jättecellsarterit från de som inte har jättecellsarterit.

I Studie IV gjordes tomografiskt 3D ultraljud på tinningkärl hos friska individer och på patienter med misstänkt jättecellsarterit. Tomografisk 3D ultraljud har tidigare använts för att visualisera kärl med goda resultat, men det har inte använts på tinningkärlet förut. Tinningkärlet undersöktes med tomografiskt 3D ultraljud och kärlväggskvoten (tjockleken på kärlväggen dividerat med hela kärldiametern) räknades ut. Tinningkärlet kunde tydligt visualiseras med tomografiskt 3D ultraljud och hög kärlväggskvot indikerade kärlväggsförtjockning, som kan tyda på jättecellsarterit.

I Studie V undersöktes hur mycket vävnadsprovet av tinningkärlet krymper efter att det skurits ut (excision) och efter att det legat i formalin (formalinfixering), vilket är tillvägagångssättet innan vävnadsprovet undersöks mikroskopiskt. Det saknas konsensus kring hur långt vävnadsprovet skall vara vid diagnostik av jättecellsarterit och det är oklart om längden som ibland rekommenderas (minst en centimeter) avser innan eller efter excision och formalinfixering. Studier har visat att biopsier av tinningkärlet kan krympa, men ingen har tittat på när biopsin krymper mest. Den diagnostiska träffsäkerheten för jättecellsarterit kan variera med längden på biopsin och eftersom biopsierna användes som diagnostisk referens i våra studier på jättecellsarterit, ville vi säkerställa att en adekvat biopsilängd togs. Resultaten visade att biopsin krympte enbart direkt efter excision och inte efter formalinfixering. Därmed kan kirurgen vara säker på att den längd på kärlbiopsin som man mäter direkt efter excision är den som kommer att analyseras mikroskopiskt avseende förekomst av inflammation.

Sammanfattningsvis är PAI, ultraljud CFS och tomografiskt 3D ultraljud lovande icke-invasiva undersökningstekniker för framtida diagnostik av jättecellsarterit. En icke-invasiv och träffsäker diagnostik, där patienten slipper att ta ett vävnadsprov vore av

stort värde. Med dessa tekniker kan hela tinningkärlets förlopp undersökas och förhoppningsvis även andra kärl som kan drabbas vid jättecellsarterit. En snabb och säker diagnos är avgörande för att kunna erbjuda fler patienter rätt behandling i tid och därmed förhindra svåra komplikationer av sjukdomen, men samtidigt även undvika att de patienter som inte har jättecellsarterit behandlas i onödan. Därtill är förhoppningen att teknikerna skall kunna användas för att följa behandlingseffekten vid jättecellsarterit, vilket kan vara en utmaning. Det krävs dock ytterligare forskning och teknikutveckling innan PAI, ultraljud CFS och tomografiskt 3D ultraljud kan användas kliniskt på våra sjukhus.

Papers included in this thesis

This thesis is based on the following five papers, which will be referred to in the text as Studies I-V.

I. Sheikh R, Hammar B, **Naumovska M**, Dahlstrand U, Gesslein B, Erlöv T, Cinthio M, Malmsjö M. Photoacoustic imaging for non-invasive examination of the healthy temporal artery – systematic evaluation of visual function in healthy subjects. *Acta Ophthalmol.* 2021 Mar;99(2):227-231.

II. **Naumovska M**, Merdasa A, Hammar B, Albinsson J, Dahlstrand U, Cinthio M, Sheikh R, Malmsjö M. Mapping the architecture of the temporal artery with photoacoustic imaging for diagnosing giant cell arteritis. *Photoacoustics.* 2022 Jul 4;27:100384.

III. **Naumovska M**, Sheikh R, Albinsson J, Hammar B, Dahlstrand U, Malmsjö M, Erlöv T. Ultrasound centre frequency shifts as a novel approach for diagnosing giant cell arteritis. *Scand J Rheumatol.* 2023 Jul;52(4):424-431.

IV. **Naumovska M**, Dahlstrand U, Engqvist L, Cinthio M, Albinsson J, Sheikh R, Merdasa A, Malmsjö M. Tomographic ultrasound for three-dimensional visualization of temporal arteries. *Scand J Rheumatol*. 2024 Mar 4:1-4.

V. **Naumovska M**, Sheikh R, Engelsberg K, Blohme J, Hammar B, Malmsjö M. Temporal artery biopsies contract upon surgical excision, but do not shrink further during formalin fixation. *Scand J Rheumatol.* 2020 Jan;49(1):84-86.

Abbreviations

3D	Three-dimensional
ACR	American College of Rheumatology
BSR	British Society for Rheumatology
CFS	Center frequency shift
CRP	C-reactive protein
CT	Computer tomography
ESR	Erythrocyte sedimentation rate
EULAR	European League Against Rheumatism
FDG-PET	^{18}F-fluorodeocyglucose positron emission tomography
GCA	Giant cell arteritis
MRI	Magnetic resonance imaging
PA	Photoacoustic
PAI	Photoacoustic imaging
ROI	Region of interest
TAB	Temporal artery biopsy

1 Introduction

Giant cell arteritis (GCA), also known as temporal arteritis, is a treatable, but potentially sight-threatening form of systemic vasculitis (1). Early and correct diagnosis are important as immunosuppressant treatment can prevent sudden irreversible blindness and other vascular events (2, 3).

GCA is typically confirmed after histopathological examination of a temporal artery biopsy (TAB) specimen. Positive biopsy findings have high specificity, but the results can be false negative in up to 15-30% of patients with GCA (4-7). Furthermore, TAB is associated with surgical risks (8, 9). A non-invasive technique for the diagnosis of GCA would therefore be of considerable benefit. Previous attempts to find alternative non-invasive diagnostic tools to replace TAB have proved inadequate for various reasons (10).

The aim of the work presented in this thesis was to evaluate three novel non-invasive techniques for future GCA diagnosis: photoacoustic imaging (PAI), ultrasound center frequency shift (CFS), and tomographic three-dimensional (3D) ultrasound.

1.1 Giant cell arteritis

1.1.1 Anatomy of the superficial temporal artery

The superficial temporal artery is a type of muscular artery consisting of three layers: the tunica intima, tunica media, and tunica adventitia (11). The internal elastic lamina separates the tunica intima and the media, and the external elastic lamina separates the tunica media and the adventitia (Figure 1). Each layer exhibits specific characteristics. The tunica intima is the innermost layer, and is composed of endothelial cells. This layer is in direct contact with the bloodstream, facilitating the exchange of nutrients, oxygen, and waste products. The tunica media is the middle layer, and is primarily composed of smooth muscle cells, responsible for regulating the artery's diameter and blood flow. Elastic fibers and collagen are also present in the tunica media. The outermost layer, the tunica adventitia, consists of connective tissue containing collagen fibers, fibroblasts, blood and lymphatic vessels, nerves, and immune cells. Fibroblasts are the most abundant cell type in the tunica adventitia. These, together with other resident adventitial cells, are thought to be the first to be activated by pathological mechanisms, such as inflammation (12). The tunica adventitia also provides structural support to the artery, and it is here that the vasa vasorum, a network of small blood vessels that supplies the arterial wall, is found.

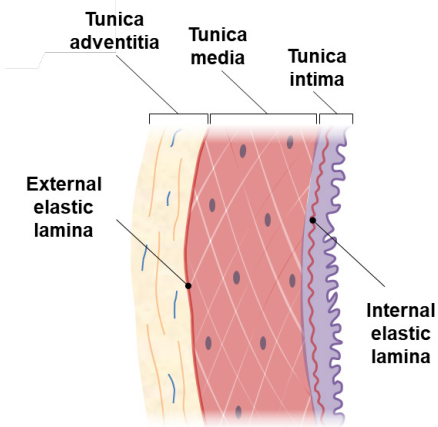

Figure 1. Anatomy of the superficial temporal artery, consisting of three layers: the tunica intima, tunica media, and tunica adventitia. The internal and external elastic laminae separate the layers from each other. Each layer exhibits specific characteristics.

The superficial temporal artery is one of the terminal, major branches of the external carotid artery (13). During its course, it gives off several branches that supply different areas of the face and scalp (Figure 2). The artery courses anteriorly, passing through the parotid gland, before dividing into the frontal and parietal branches above the zygomatic arch (14), where it lies close to the facial nerve (15). Anatomical variations exist, consisting mainly of supplementary branches (16, 17).

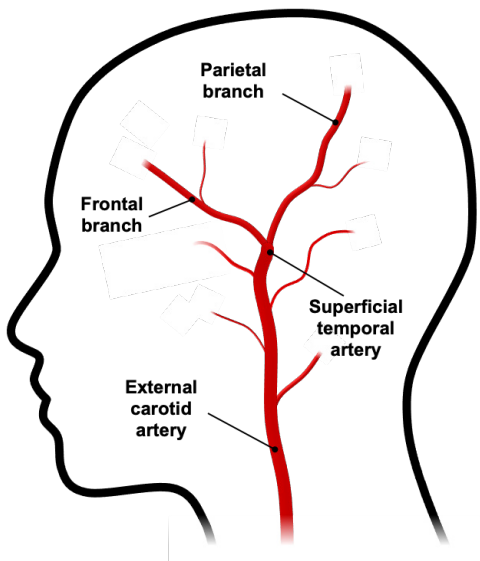

Figure 2. Vascular anatomy of the superficial temporal artery and its branches. Anatomical variations are found between individuals, in particular in its branching pattern.

The mean diameter of the superficial temporal artery at the zygomatic arch has been estimated to be 2.2-2.7 mm (16-18) and decreases distally (18). The length of the frontal and parietal branches varies between individuals, but both are approximately 10 cm measured from above the upper margin of the zygomaticus, based on digital subtraction angiography (18).

1.1.2 Epidemiology and pathology of GCA

GCA is the most common form of primary vasculitis in patients aged ≥50 years, affecting arteries of medium and large size, with a predilection for the cranial arteries, such as the superficial temporal artery (8, 19). One of the earliest documented observations of GCA dates back to the 10th century by the ophthalmologist Ali Ibn Isa of Baghdad, who described an association between inflamed arteries and visual symptoms (1). The first description of the clinical features of GCA was then given by Hutchinson in 1890, but a more comprehensive report did not emerge until 1932, when Horton obtained the first TAB and performed histological evaluation (20).

GCA affects individuals over the age of 50 years, the average age of presentation being 75 years, with a significant increase in incidence with advancing age (21, 22). It is extremely rare before the age of 50 years (23). GCA is more frequently diagnosed in women than in men, with a female-to-male ratio estimated to be around 3:1 (24, 25). The incidence of GCA varies geographically, and higher rates are reported in populations of Northern European descent, such as Scandinavians (26, 27). A meta-analysis reported an overall pooled incidence of GCA of 10.0 per 100,000 in people aged ≥50 years (28). Notably, Scandinavia exhibited the highest incidence at 21.6 per 100 000, followed by North and South America, Oceania and Europe. This suggests a potential role of environmental factors, but genetic factors may contribute, as specific HLA alleles, particularly HLA-DRB1*04, have been associated with increased susceptibility (29, 30). A decrease in the incidence rate of biopsy-proven GCA has been observed in Sweden but also in other parts of the world (22). Possible explanations may be linked to the use of alternative diagnostic techniques besides TAB, changes in environmental factors, or could signify a genuine decrease in the incidence of GCA.

GCA is considered an autoimmune disorder and the pathogenesis of GCA involves complex immune-mediated processes. While the exact cause remains unclear, several key aspects of its pathophysiology have been identified. Unknown stimuli activate immature dendritic cells in the adventitia through toll-like receptors, leading to chemokine release, which recruits CD4(+) T cells with IL-6 release (31). Under the influence of IL-6, these cells differentiate into Th1 and Th17 cells leading to the release of IFN-γ and IL-17. These cytokines recruit monocytes that transform into macrophages, enabling the formation of multinucleated giant cells, and promote the proliferation of vascular smooth muscle cells, leading to luminal stenosis. In contrast, the number of regulatory T cells, which normally serve to limit immune response, is decreased (32). T cells and macrophages also form granulomatous infiltrates in the adventitial and medial layers of the affected artery (33). The center of tissue damage lies

at the intima–media junction close to the internal elastic lamina and at the border between the media and adventitia (34).

Despite its systemic character, GCA does not affect all arteries. The most frequently involved arteries are branches of the external carotid artery and the posterior ciliary arteries that supply the optic nerve, but also the aorta and its upper extremity branches (8, 35, 36).

1.1.3 Symptoms and complications of GCA

GCA is a heterogeneous disease with more than one clinical picture, and the spectrum of GCA encompasses overlapping phenotypes, making its diagnosis challenging (3). The clinical features depend on which artery is affected. GCA is generally regarded as a form of cranial arteritis, but may also present as large-vessel vasculitis, or single-organ arteritis (37). The prevalence of large-vessel vasculitis is thought to be high: about 15-30% of patients with GCA have radiographic evidence of the involvement of the aortic trunk and its branches (38, 39). In other studies, the axillary arteries were found to be affected in up to 50% of patients (40, 41). However, cranial arteries are believed to be almost always involved (36, 42).

The symptoms of GCA may vary between individuals. Typical symptoms of cranial involvement are headache, scalp tenderness, and jaw claudication (10, 43). Headache is the most common symptom, found in 2/3 of patients with GCA, and can vary in onset, intensity, and character. It is often associated with scalp tenderness and tenderness over the temporal artery. A new onset or changed pattern of headache in an individual aged over 50 years should always raise suspicion of GCA. Pain in the tongue or in the jaw upon chewing is also common and is seen in half of patients with GCA (10).

Many patients with GCA report systemic features such as malaise, fatigue, fever, night sweats, and weight loss, and these are believed to be secondary to cytokine release (43, 44). GCA presents with these non-specific symptoms in 40% of cases (45). In cases of large-vessel vasculitis, patients can experience symptoms such as arm claudication, diminished or absent pulse in the arms, and signs of aortitis (10).

GCA is often associated with polymyalgia rheumatica which is seen in 40-60% of patients with GCA (10). Symptoms of polymyalgia rheumatica include muscle pain and stiffness, particularly in the shoulders, neck, and hips.

Visual complications occur in about 10-15% of cases (2, 46-48), and constitute the most feared aspects of GCA, but are uncommon once corticosteroid treatment has been initiated (48). Early and appropriate corticosteroid therapy is effective in preventing further visual loss in the majority of patients experiencing visual complications due to GCA (49). Untreated patients with unilateral visual loss have up to 50% risk of blindness in the other eye, usually occurring after a few days (50, 51), most often secondary to anterior ischemic optic neuropathy (Figure 3). Other visual complications include central retinal artery and cilioretinal artery occlusion, amaurosis fugax, diplopia, posterior ischemic optic neuropathy, and choroidal infarction (49).

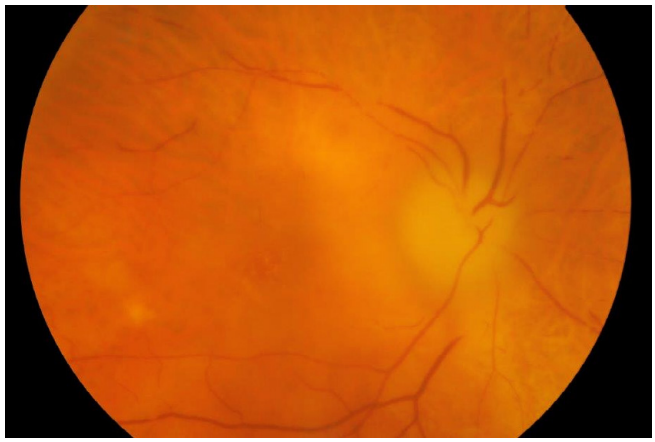

Figure 3. Image of arteritic anterior ischemic optic neuropathy. Note the pale papillary edema, which should raise suspicion of an arteritic cause.

Some patients experience occult GCA, that is, visual complications without other symptoms of GCA, although levels of C-reactive protein (CRP) and/or erythrocyte sedimentation rate (ESR) can be elevated. Occult GCA has been reported to occur in up to 21.2% of patients with GCA (52). Other complications, although uncommon, are stroke (53), aortic dissection, aortic aneurysm (thoracic or abdominal), and large artery stenosis (54).

1.1.4 Treatment of GCA

Given the potential for severe complications, early diagnosis and treatment of GCA are critical to prevent vision loss and other complications, but also to reduce inflammation and alleviate symptoms (2, 3). The recommendation is to initiate immediate treatment with high-dose corticosteroids (55), followed by diagnostic confirmation. This treatment is associated with a number of side effects such as diabetes, osteoporosis, weight gain, increased susceptibility to infections and Cushingoid symptoms, and usually extends over a long period of time, up to several years (3). Most patients achieve drug-free remission 2-3 years after disease onset (22). Correct diagnosis is therefore important to prevent patients who do not have GCA from being treated unnecessarily for an extended period.

In long-term management, methotrexate, an immunosuppressive agent, can be used to reduce the dose of corticosteroids, or as an addition to corticosteroid taper in relapsing GCA (55). Tocilizumab, a monoclonal antibody targeting the IL-6 receptor, is an alternative addition to corticosteroid taper in refractory or relapsing GCA or as a steroid-sparing treatment (56). Treatment with tocilizumab, combined with corticosteroids, offers a higher likelihood of sustained remission and a reduced cumulative corticosteroid dose compared to treatment with corticosteroids alone (57).

1.2 Diagnostic evaluation of GCA

The final diagnosis of GCA is usually based on the combination of several parameters, as described below.

1.2.1 Laboratory testing

The diagnostic evaluation of GCA often begins with measurement of the ESR. In one study, the ESR was elevated in the majority of patients, giving a mean value of 85 mm/hour (58), but the ESR has been found to be normal in up to 24% of cases of GCA (58-60). The combination of elevated ESR and CRP improves the specificity of the diagnosis of GCA, and both markers are normal in only 2.4-4% of biopsy-proven cases of GCA (39, 61). Other laboratory findings include normochromic anemia, and elevated levels of thrombocytes and leukocytes (46).

1.2.2 Temporal artery biopsy

TAB is currently considered the gold standard in the diagnosis of GCA (62), where a segment of the temporal artery is surgically excised and examined histopathologically (Figure 4). This technique has high specificity but low sensitivity (7), and biopsy findings can be negative in 15-30% of patients with GCA (4-6). This may be due to discontinuous inflammation (so-called skip lesions) (63, 64), short biopsy specimens (65), low number of histological sections, long duration of corticosteroid treatment prior to biopsy (66), or no involvement of cranial arteries (41). Furthermore, surgical biopsy is an invasive procedure and is associated with surgical risks, e.g. injury to the facial nerve, peri- and postoperative hemorrhage, and wound infection (8, 9). In a study from southern Sweden, the annual rate of performing a new TAB was 64.1 per 100 000 individuals aged ≥50 years during the 23-year study period (22). Of these biopsies, 20% were positive for GCA, indicating that GCA is suspected far more frequently than it is diagnosed with TAB.

Biopsy findings remain positive for at least 2-6 weeks after commencement of treatment with corticosteroids (67, 68), although histologic findings of GCA start to change earlier (69). The diagnostic accuracy of TAB is, however, greater the earlier TAB and histopathological evaluation are performed after the start of treatment. The diagnostic yield within four weeks of starting high-dose corticosteroid treatment has been shown to be 74%, but only 40% beyond this period (66).

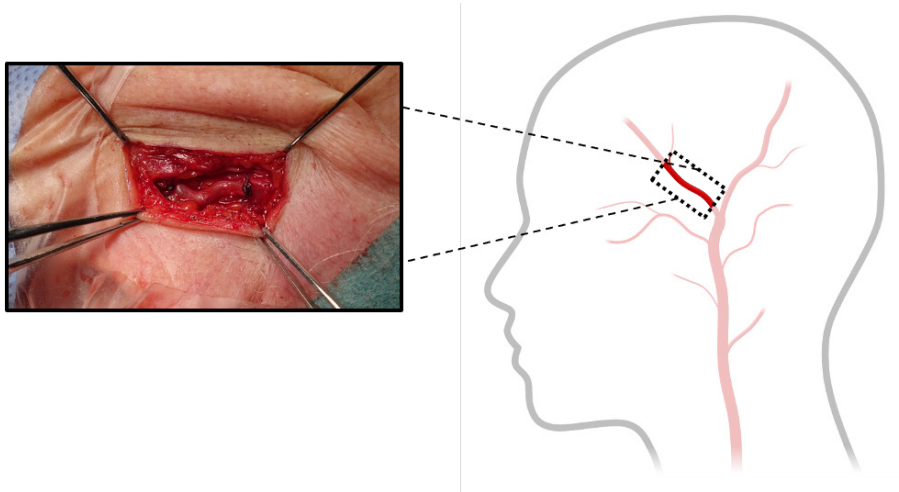

Figure 4. Surgical excision of a temporal artery biopsy specimen under local anesthesia.

Histopathological findings in GCA

Typical histopathological findings in GCA are transmural cell infiltrates composed of lymphocytes, macrophages, and multinucleated giant cells, intimal hyperplasia, internal elastic lamina disruption or fragmentation, and focal areas of intimal and medial necrosis (70) (Figure 5). Giant cells are multinucleated cells formed by the fusion of macrophages, and are often seen close to the internal elastic lamina. They are present in about one-half of positive biopsies (33). Granulomas are often present in the arterial wall, constituting localized areas of chronic inflammation, consisting of aggregates of immune cells, particularly macrophages. Granulomas are often localized in the medial and adventitial layers. The vasa vasorum can also be affected by inflammation. Chronic inflammation in GCA can further lead to arterial wall remodeling, including fibrosis.

The extent of inflammation in the artery varies. Inflammation is often segmental, and the degree of inflammation ranges from slight adventitial infiltrates to fully developed granulomatous lesions distributed along the entire vessel wall (71).

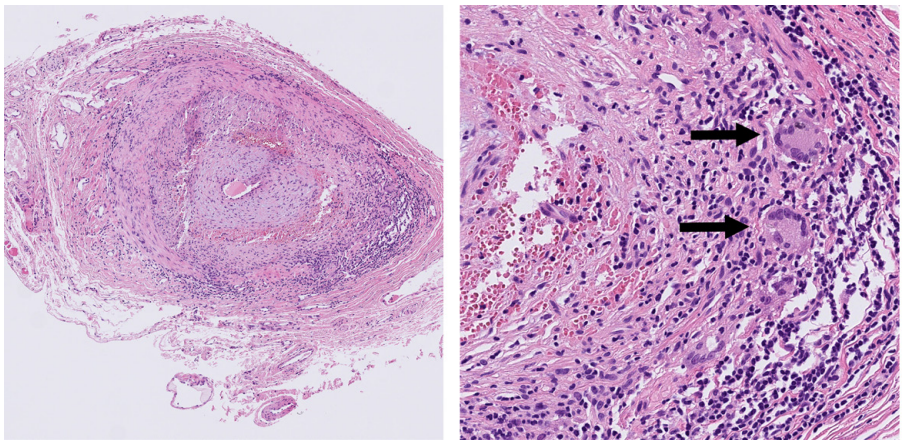

Figure 5. Histopathological sections of a temporal artery from a patient diagnosed with giant cell arteritis, stained with hematoxylin-eosin, showing the infiltration of inflammatory cells, thickening of the tunica intima, and multinucleate giant cells (black arrows).

Temporal artery biopsy length

In order to minimize the risk of false-negative findings in histopathological evaluation, it has been suggested that the biopsy must be sufficiently long (65, 72-75). However, the required length of the TAB to ensure adequate diagnostic sensitivity is the subject of debate.

Several studies have reported comparable biopsy lengths in arteries with and without inflammatory lesions (6, 76, 77), whereas others have found that in subjects with histologically detected inflammation, the artery specimens were significantly longer (65, 72, 74, 75). However, it has also been shown that there is a correlation between systemic inflammation and reduced arterial elasticity in vasculitis in other parts of the body (78, 79). In a study on patients with TAB findings positive for GCA, it was suggested that contraction of the biopsy after excision was less in the inflamed arteries (80). This raises the question of whether the difference in length between positive and negative TABs is due to greater contraction of the negative specimens, rather than an indication that the biopsy length is generally longer in positive TABs. It has also previously been claimed that the specimen length is of minor importance, and that the histopathologic evaluation of thin sections by an experienced pathologist is of greater value (81).

Thus, the length of the TAB specimen yielding the best diagnostic accuracy is still the subject of discussion. A large multicenter study indicated that a TAB length of 0.5 cm could be sufficient (77), while in another study, a post-fixation length of at least 1 cm was suggested (72), as is the recommendation in the latest guidelines issued by the British Society for Rheumatology (BSR) (55). However, surgical specimens of other human tissues (e.g. skin tumors) are known to contract as a result of the retractile properties of the tissue and the action of formalin (82, 83), and this has also been reported in the case of TAB (80, 84-86). Since the sensitivity of diagnosis by TAB may

vary with biopsy length (74, 87), the degree of tissue contraction has clinically important implications as the specimen length is determined before excision. To the best of the author's knowledge, no studies have been published in which the effects of both surgical excision and formalin fixation on TAB specimens have been investigated. This was explored in the present work in Study V.

1.2.3 Clinical predictive models for GCA

GCA is often diagnosed based on the combination of various clinical parameters, laboratory testing and the result of histopathological examination of the TAB specimen (67). There are to date no specific diagnostic criteria for GCA (10, 61). The 1990 American College of Rheumatology (ACR) criteria for the classification of GCA (88) may assist in diagnosing GCA, but these were intended to distinguish patients with GCA from those with other forms of vasculitis, and cannot be used for the diagnosis of GCA in individual cases (89, 90). Therefore, the classification criteria should only be applied when a diagnosis of large vessel or medium vessel vasculitis have been made. The ACR criteria require the fulfilment of three out of five core features, being age 50 years or older at onset, a new headache, clinical temporal artery abnormality, elevated ESR of at least 50 mm/hour, and an abnormal TAB (88). However, these criteria were established before the widespread use of vascular imaging modalities, which have been increasingly incorporated in the clinical assessment of GCA. Also, the 1990 ACR criteria focus mainly on cranial features of GCA and do not perform well in classifying with disease predominantly affecting the larger arteries. In 2022, the criteria were updated and the 2022 ACR/European League Against Rheumatism (EULAR) classification criteria for GCA incorporate the use of imaging modalities, such as ultrasound (23).

Previous studies have investigated predictive variables that could be used to estimate the probability of a TAB being positive for GCA (4, 91, 92). In one study, increased thrombocytes, CRP and ESR, jaw claudication, vision loss, headache, and clinical temporal artery abnormality were found to be statistically significant positive predictors of a positive TAB (92). Similar results were reported by Duhaut et al. (91). Gonzalez-Gay et al. found that the best predictive model of biopsy-proven GCA included a history of constitutional syndrome (asthenia, anorexia and weight loss), an abnormal temporal artery upon physical examination, and the presence of visual complications (4). The presence of jaw claudication, followed by diplopia, is thought to be one of the strongest predictors of positive TAB among patients with suspected GCA (43). In another study, the combination of ESR <40 mm/hour, absence of jaw claudication, absence of temporal artery tenderness, and the presence of synovitis was found to be associated with a 95% probability of a negative TAB (93). Previous results have suggested that biopsy-negative GCA seems to be less severe than biopsy-proven GCA (91). These observations suggest that biopsy-negative GCA may be a subgroup of GCA with less ischemic complications (e.g. vision loss) and inflammatory response (less anemia and thrombocytosis, and lower ESR).

When evaluating the probability of vision loss, older age, a history of transient visual loss, jaw claudication (94), and transient diplopia (95) have been associated with an

increased risk. Another study found that low CRP and the absence of headache, fever, and palpable abnormal temporal artery were potential risk factors for visual loss (2).

The importance of using clinical parameters is highlighted by the findings in the TABUL study (Temporal Artery Biopsy vs. Ultrasound in the Diagnosis of GCA) (7). One-third of the patients eventually diagnosed with GCA had neither a positive ultrasound scan nor a positive TAB, emphasizing the importance of assessing clinical indicators to support the diagnosis.

1.3 Challenges associated with diagnosing GCA

As discussed in detail above, the diagnosis of GCA is associated with several challenges. These include the variable clinical picture of GCA, where symptoms may diverge between individuals and may often be diffuse, the lack of specific blood markers and specific diagnostic criteria for GCA, and the low sensitivity of TAB evaluation with its associated surgical risks. Safe, reliable and prompt diagnosis would facilitate early treatment of GCA, which is of great importance as this can prevent vision loss and other complications. An accurate diagnosis would also prevent patients who do not have GCA from being treated unnecessarily, thereby avoiding side effects associated with this treatment, as well as unnecessary healthcare costs. This emphasizes the need for alternative diagnostic methods.

1.4 Current non-invasive diagnostic techniques for GCA

In recent years, imaging modalities have become integral components of the diagnostic assessment for GCA, supported by the 2018 EULAR recommendations regarding the use of imaging in large vessel vasculitis (96). A few non-invasive vascular imaging techniques have been investigated or are being used to obtain complementary information for the diagnosis of GCA. These have some advantages, but also disadvantages, such as the use of contrast agents, exposure to ionizing radiation, poor usability, low resolution, or a combination of these.

1.4.1 Ultrasound

Conventional ultrasound, such as B-mode ultrasound and color Doppler ultrasound, has been used extensively for the examination of cranial and extracranial arteries in suspected GCA and offers the advantages of widespread availability and no radiation exposure. Generally, previous studies have reported good specificity (82-93%), but lower sensitivity (68-76%), in diagnosing GCA when examining the temporal arteries (97-101), with a broad range of sensitivity among studies. The variability in sensitivity

is mostly due to differences in, for example, the degree of operator experience and the choice of reference standard for the diagnosis of GCA (usually biopsy or ACR criteria). Ultrasound is highly dependent on the operator's experience and is susceptible to misleading artifacts if not applied by trained experts using the appropriate equipment (102). Some studies have thus found that conventional ultrasound has high sensitivity and specificity in diagnosing GCA, when carried out by experienced ultrasound operators (103-106).

The most common signs on ultrasound indicating GCA are a dark halo around the arterial lumen, called the halo sign, and vascular stenosis or occlusion. The halo sign is thought to be caused by edema in the artery wall (98, 104) and is the most specific ultrasound finding for GCA (98) (Figure 6). According to a meta-analysis in 2010 (97), a unilateral halo sign has a sensitivity of 68% and a specificity of 91%. However, the TABUL study, the purpose of which was to determine the diagnostic accuracy of ultrasound of the temporal artery and the axillary artery in comparison to TAB in the diagnosis of GCA, demonstrated lower values of 54% sensitivity and 81% specificity (7). This is probably due to operator dependence, as the halo sign can easily be missed or erroneously diagnosed when applying inappropriate ultrasound settings (107). The sensitivity of ultrasound can, however, be further improved by examining larger vessels (common carotid arteries and axillary arteries) in addition to the temporal arteries (108). Studies investigating both cranial and extracranial arteries have shown consistently higher sensitivities than those focusing on temporal arteries only (109).

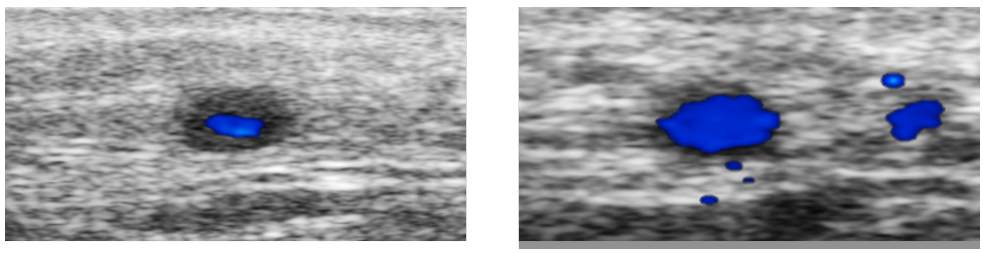

Figure 6. The halo sign (left image), a dark halo around the arterial lumen, seen upon examination of the temporal artery using color Doppler ultrasound. It is thought to be caused by edema in the artery wall due to inflammation, and is the most specific ultrasound finding for giant cell arteritis. The right image illustrates a transverse ultrasound scan of a healthy temporal artery, where the halo sign is not observed. The blue color represents blood flow moving away from the ultrasound transducer.

Another approach using ultrasound has been suggested for the diagnosis of GCA, using the compression sign, which is positive when the vessel wall remains visible upon transducer-imposed compression of the artery, due to inflammation and arterial wall thickening (107, 110). The compression sign is thought to be less dependent on the operator's experience and has shown strong interobserver agreement (110, 111). The compression sign has been found to have a sensitivity and specificity equivalent to those of the halo sign (107).

Cut-off values of the thickness of the intima media of the temporal, facial, and axillary arteries have also been proposed to discriminate between patients with and without GCA (112). This also allows a more objective assessment of the arteries than the halo sign.

Ultrasound is associated with other limitations, apart from operator dependence. False positive results are sometimes seen as a result of atherosclerosis (113), and the sensitivity is further reduced in cases of periadventitial small-vessel vasculitis or vasa vasorum vasculitis (114, 115). Patients exhibiting these disease patterns, in contrast to a more classic transmural pattern, have a low rate of positive findings for GCA on ultrasound (114). Furthermore, the sensitivity of ultrasound imaging is significantly reduced within the first week of therapy with corticosteroids (116, 117), and the halo sign tends to disappear about two weeks after the start of corticosteroid treatment (104), although signs of inflammation caused by GCA are seen longer upon histopathological examination.

The ultrasound technique has advanced in recent years and the use of devices with improved resolution, coupled with high-frequency ultrasound probes, has facilitated a more precise assessment of cranial arteries in cases of suspected GCA (100). Depending on the clinical context, vascular ultrasound could, in some cases, be used for diagnosing GCA, provided there is a high level of expertise in ultrasound imaging and appropriate equipment is used (96). The EULAR (96) and BSR (55) guidelines have recommended ultrasound of temporal and axillary arteries as the first diagnostic test to confirm GCA. However, the ACR recently published management guidelines for GCA, stating that TAB should be the primary diagnostic test for GCA (62). Thus, there is a lack of consensus about the precise role of ultrasound in the diagnosis of GCA, and ultrasound cannot currently replace surgical biopsy and histopathological examination (37, 97), but may act as a complementary diagnostic technique.

1.4.2 Magnetic resonance imaging

High-resolution magnetic resonance imaging (MRI) has been used in several studies to assess the temporal and occipital arteries in suspected GCA with reported sensitivities of 68-89% and specificities of 73-97%, using the 1990 ACR criteria for diagnosis (37). MRI and ultrasound have also been compared directly in the diagnosis of cranial GCA, showing similar sensitivities and specificities (118). According to the latest BSR guidelines for the management of GCA, MRI of the cranial arteries may be useful in ruling out GCA if the result is negative, but should not be used as a first choice to confirm GCA (55).

An advantage of MRI is its possibility to investigate multiple vessels at the same time. Gadolinium-enhanced MRI may help to identify the presence of large-vessel involvement (119), but appears to be very sensitive to corticosteroid therapy (116). Another drawback of high-resolution MRI is its low accessibility and high cost.

1.4.3 ^{18}F-fluorodeocyglucose positron emission tomography

^{18}F-fluorodeocyglucose (FDG) positron emission tomography (PET), usually combined with low-dose computer tomography (CT), can be used to detect inflammation in extracranial vessels based on the intensity of the glucose analog uptake, and might be valuable in cases of suspected large-vessel vasculitis (120). It can also be used for differential diagnosis, as it may detect malignancy or infection (55). The disadvantages of FDG-PET/CT include high costs, limited availability, and radiation exposure.

The ability of FDG-PET to detect involvement of the aorta and its major branches has been investigated with varying results. The reported sensitivity and specificity range from 56 to 77% and from 77 to 99%, respectively (121).

FDG-PET was previously considered inadequate for the assessment of cranial arteries because of the proximity to the brain (122) . However, recent studies report that FDG-PET may detect cranial involvement in GCA with high sensitivity and specificity (96).

1.4.4 Contrast-enhanced computer tomography

Vessel wall thickening in large-vessel vasculitis due to GCA can be visualized with contrast-enhanced CT (CT/CT-angiography) (123). Although it has lower sensitivity than FDG-PET/CT, it may provide an alternative for the assessment of large-vessel vasculitis in clinics where FDG-PET/CT is unavailable (120). It is also valuable in differential diagnosis. CT/CT-angiography offers good image quality, but the intravenous injection of a contrast medium is required, and it has the disadvantage of ionizing radiation exposure. It is therefore not routinely used in the diagnostic assessment of GCA.

1.5 Novel imaging techniques

1.5.1 Photoacoustic imaging

Photoacoustic imaging (PAI) is a hybrid imaging modality that combines the strengths of optical imaging with ultrasound imaging. PAI is currently one of the most rapidly developing biomedical imaging techniques, with the capability to provide high-resolution images of biological tissues at depths of up to several centimeters (124, 125).

Previous studies using PAI have shown promising results when examining a wide range of tissues in humans (126), providing high-resolution 3D images of the structure and function of the imaged tissue. Vasculature has also been imaged effectively in animal studies (127), and in studies of human vessels, including vessels of the skin (128, 129), coronary arteries (130), carotid arteries (131), the radial artery (132), vessels of the lower extremities (133), the digital arteries (134), and vessels of the palm (135) (Figure 7).

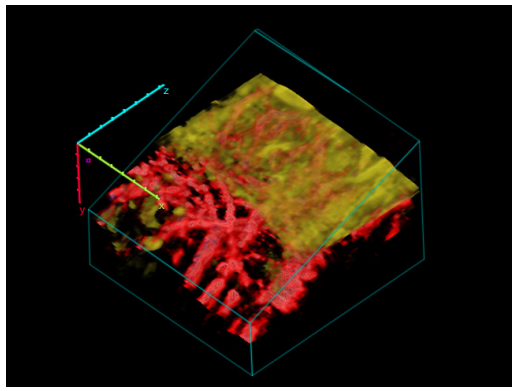

Figure 7. Image of the skin and the vascular bed from an *in vivo* examination with photoacoustic imaging of a forearm, showing melanin (yellow) and the blood vessels (red). The layer with melanin has been removed from half of the image, revealing the vascular network.

In a pilot study performed by our research group, PAI was used to examine the temporal artery to test a clinical setup for future studies, in order to identify possible challenges in the clinical setting and ways of overcoming them (136). The energy levels during PAI were measured, and safety measures were defined. The laser irradiance and the ultrasound power to which the subjects were exposed in the temporal region were found to be below the limits given in regulatory standards, and the PAI setup was therefore determined to be safe. However, no detailed investigation of safety regarding visual function or patient tolerability was carried out, nor was the spectral information from the temporal artery systematically analyzed.

No clinical studies have previously been performed to evaluate PAI of the temporal artery wall and its suitability for diagnosing GCA. In Study I, the safety of PAI in humans was evaluated and the spectral signature of the healthy temporal artery *in vivo* was defined. In Study II, the ability of PAI to map the temporal artery *ex vivo*, in subjects with suspected GCA, was assessed.

1.5.2 Ultrasound center frequency shift

Ultrasound CFS is a novel ultrasound technique based on the shift in center frequency of the ultrasound radio frequency data (the raw data obtained from ultrasound scanning), and provides an objective measure of microstructures in the tissue. Ultrasound CFS has shown promising results in identifying lesion components contributing to increased plaque vulnerability in carotid arteries and the risk of vascular events such as stroke (137). In the work presented in this thesis, the ability of ultrasound CFS to discriminate between GCA-positive and GCA-negative biopsies was assessed (Study III).

1.5.3 Tomographic 3D ultrasound

Tomographic 3D ultrasound is an electromagnetically tracked system that enables the objective documentation of tissues in a single free-hand sweep. The technique works through video capture and can be coupled to commercially available ultrasound systems.

Tomographic 3D ultrasound has already proven useful and reliable for measuring vessel geometry (138) and, for example, in assessing vessel stenosis (139), carotid plaque volume (140) and abdominal aorta aneurysm (141), but has not been evaluated with regard to its ability to visualize and measure geometric features in temporal arteries. This was assessed in Study IV.

1.6 Thesis at a glance

The studies described in this thesis are summarized below.

Study	Aim	Method	Subjects (n)	Setting
I	To confirm the safety and patient tolerability of PAI, and to define the spectral signature of the healthy temporal artery	PAI	Healthy (12)	*In vivo*
II	To map the temporal artery and to evaluate the feasibility of differentiating between GCA-positive and GCA-negative biopsies	PAI	Suspected GCA (77)	*Ex vivo*
III	To evaluate the feasibility of discriminating between GCA-positive and GCA-negative biopsies	Ultrasound CFS	Suspected GCA (68)	*Ex vivo*
IV	To visualize the temporal artery and to calculate vessel dimensions	Tomographic 3D ultrasound	Suspected GCA + healthy (17)	*In vivo*
V	To evaluate the effect of surgical excision and formalin fixation on TAB length, and to compare the results obtained from GCA-positive and GCA-negative biopsies	Measuring TAB length	Suspected GCA (28)	*In vivo*, *ex vivo*

2 Aims

The aim of this work was to evaluate PAI, ultrasound CFS and tomographic 3D ultrasound for future application in the non-invasive diagnosis of GCA. These techniques were assessed on human temporal arteries, *in vivo* or *ex vivo*.

The specific aims were:

- to study patient tolerability and safety regarding visual function when using PAI, and to define the spectral signature of the healthy temporal artery (Study I),
- to study the ability of PAI to map the temporal artery and to evaluate the feasibility of differentiating between GCA-positive and GCA-negative biopsies (Study II),
- to study the feasibility of ultrasound CFS to discriminate between GCA-positive and GCA-negative biopsies (Study III),
- to study the ability of tomographic 3D ultrasound to visualize the temporal artery and to measure artery dimensions (Study IV), and
- to study the effect of surgical excision and formalin fixation on TAB length, and to compare the results obtained from GCA-positive and GCA-negative biopsies (Study V).

3 Methods

3.1 Ethics

All the subjects participating in the studies described in this thesis were recruited at the Department of Ophthalmology, Skåne University Hospital, Lund, Sweden. The subjects were given information about the study and the voluntary nature of participation. All subjects gave their informed written consent before participation. The protocol for the studies was approved by the Ethics Committee in Lund, Sweden, or the Swedish Ethical Review Authority, and complied with the principles of the Declaration of Helsinki as amended in 2008.

3.2 Photoacoustic imaging

3.2.1 The principles of photoacoustic imaging

PAI employs a combination of laser light and ultrasound, offering better spatial resolution at greater depths than purely optical imaging modalities. By using a combination of laser light and ultrasound, PAI takes advantage of the low acoustic scattering in tissue and the fact that sound scatters 1000 times less than light (126). Thus, the acoustic signal propagates much deeper in biological tissue without significant scattering, which enables optical contrast imaging at far greater depths (125). Another advantage of PAI is that it is less user-dependent, since the spectral signature obtained is an objective measure.

In PAI, a laser unit emits non-ionizing nanosecond pulses of different wavelengths within the near-infrared light spectrum into the tissue, which absorbs the energy from the laser pulses (142). This leads to a slight increase in temperature, causing thermoelastic expansion that generates acoustic waves, which are detected by an ultrasound transducer and then converted into a multispectral image. This enables high-resolution 3D images to be obtained, reflecting the molecular composition of the tissue.

PAI is mainly based on endogenous contrast, that is, the intrinsic optical absorption of tissue chromophores such as hemoglobin, melanin, lipids, and water. These chromophores exhibit characteristic absorption spectra, and PAI at multiple wavelengths allows their relative quantification. Thus, the spectral photoacoustic (PA) signal of each pixel in the image is derived from the absorption of light by the

endogenous chromophores of the tissue. Various exogenous contrast agents can also be employed, such as dyes or nanoparticles, for better contrast and deeper imaging (143).

3.2.2 Photoacoustic equipment

In Studies I and II, PAI was performed using a Vevo LAZR-X imaging system (FUJIFILM VisualSonics Inc., Toronto, ON, Canada). This system is equipped with an ultrasound linear array transducer and a fiberoptic bundle, which are coupled to a 20-Hz tunable laser with a nanosecond pulse duration. The laser can be operated in two wavelength ranges: 680-970 nm and 1200-2000 nm. In the studies presented in this thesis, the 680-970 nm wavelength range was used to image the temporal artery.

During PAI, ultrasound is used as a guide and the ultrasound scans are interleaved with the laser pulses. Two planar light beams, located on either side of the ultrasound linear array, illuminate the target area (Figure 8). A 10-mm-thick Aquaflex ultrasound gel pad with protective plastic film was used to achieve an adequate distance between the laser fibers and the skin (Study I), or the TAB specimens (Study II), the latter to mimic a future *in vivo* setup. Ultrasound gel was used to achieve good acoustic coupling between the transducer and the skin surface (Study I). The photoacoustic waves were detected using an MX400 ultrasound linear array transducer from VisualSonics Inc. This transducer has a central frequency of 30 MHz and a bandwidth of 22-55 MHz, which provide axial and lateral resolutions of 110 µm and 50 µm, respectively.

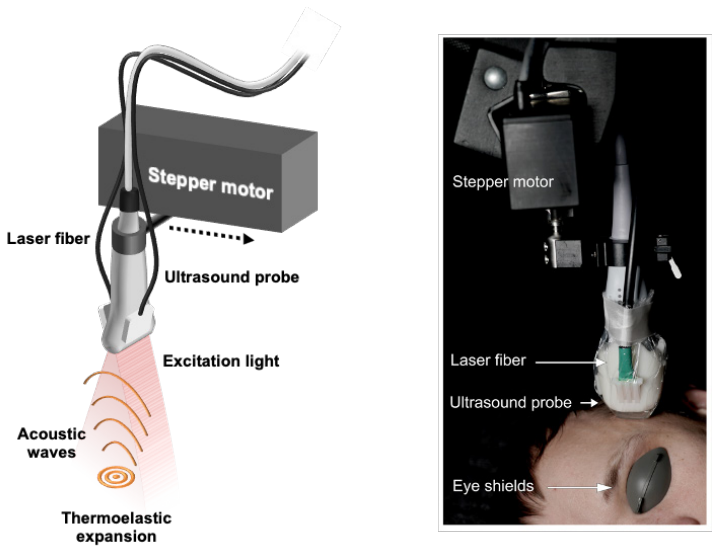

Figure 8. Illustration of the photoacoustic imaging setup (left) and the image from an *in vivo* examination (right). The photoacoustic probe consists of an ultrasound transducer with laser fiberoptic bundles attached on each side, which is fixed to an adjustable arm with a linear stepper motor to scan the whole target. The tissue is irradiated with pulsed laser light, causing thermoelastic expansion, which generates acoustic waves that can be detected by the ultrasound transducer.

The transducer was fixed to an adjustable arm to prevent motion artifacts caused by the examiner and was driven by a linear stepper motor to allow 2D multispectral images to be collected with a step size of 0.5 mm. In this way, 3D hybrid images of ultrasound and photoacoustic waves were obtained.

3.2.3 Safety aspects

Safety regulations were followed as described previously by our research group (136). The windows and doors in the examination room were covered, and protective eye shields, in combination with black aluminum foil, were worn by the study subjects throughout the examination. Block-out glasses were worn by the staff.

The laser irradiance and the ultrasound power to which the subjects were exposed in the temporal region have previously been determined (136) and were well below the laser safety levels given in IEC 60825-1 (144), and the ultrasound safety level required by the FDA (145) and the British Medical Ultrasound Society (146).

3.2.4 Photoacoustic imaging of healthy temporal arteries (*in vivo*) and of biopsies from cases of suspected GCA (*ex vivo*)

The aim of Study I was to confirm patient tolerability and safety regarding visual function when using PAI, and to define the spectral signature of the healthy temporal artery *in vivo*. Twelve subjects were included, who were interviewed and clinically examined by the same medical doctor. Visual function was tested before and after PAI examination, and included visual acuity, color vision, and visual field. Best corrected visual acuity was measured with the Snellen letter chart (Ortho-KM, Lund, Sweden), color vision was tested with both Sahlgren's Saturation Test (VISUMETRICS AB, Göteborg, Sweden) and the Ishihara color vision test (Luxvision, US Ophthalmic, Doral, USA), which allows discrimination between congenital and acquired defects (147), and the visual field was measured with a Humphrey visual field analyzer, using the 24–2 test protocol (Carl Zeiss Meditec AG, Jena, Germany). The subjects' experience of the PAI examination was assessed using a visual analog scale ranging from 0 to 100, and included the level of discomfort, heat sensation from the probe, and light sensation.

The aim of Study II was to map the temporal artery in cases of suspected GCA, and to test the feasibility of differentiating between photoacoustic spectra from biopsies assessed as positive and negative for GCA. Patients with suspected GCA undergoing TAB were assessed for eligibility to participate in the study, and 77 patients were included. TAB was performed under local anesthesia according to local practice, and the biopsy was then placed in balanced saline solution (BSS). Blood was removed from the vessel by rinsing the lumen with BSS, using a hypodermic needle and a syringe. Surgical threads were sewn to each end of the biopsy, and it was then placed in a 100 × 70 × 50 mm^3 Perspex container filled with BSS, with a layer of black ultrasound-attenuating material in the bottom (Figure 9). The biopsy was held in place by the surgical threads. After PAI scanning, the TAB specimens were placed in formalin and

sent for histopathological examination for signs of inflammation compatible with GCA. Thirty-six of the biopsies were assessed as positive for GCA and 41 biopsies were negative.

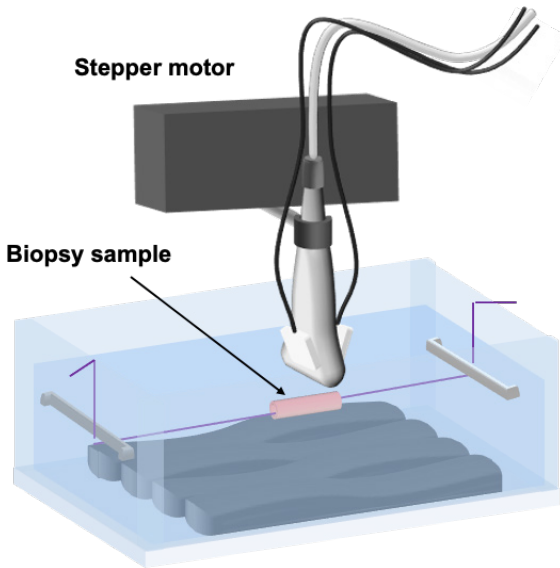

Figure 9. The photoacoustic scanning setup used to examine the biopsy samples. The sample is mounted in a container filled with balanced saline solution, with an ultrasound-attenuating material in the bottom. The transducer is fixed to an adjustable arm and is driven by a linear stepper motor.

Photoacoustic scanning in vivo *and* ex vivo

In Studies I and II, 59 excitation wavelengths were used over a broad spectral range (680-970 nm), which provides detailed absorption spectra of the different tissue chromophores.

The temporal artery was first analyzed with PAI on multiple wavelengths, in which multispectral PA images were collected from 680 to 970 nm in 5-nm increments to obtain spectral signatures of the tissue. This generates 59 unique PA images (one for each wavelength), or one multispectral PA image. Thus, each pixel in the image contains a single spectrum dependent on the optical properties of the tissue, and how photons of different energies are absorbed. The length of the imaged artery determined how many of these measurements could be made, but the number was approximately three to four per artery.

A photoacoustic scan was then performed using the stepper motor, starting with a single wavelength scan at 820 nm for initial control of the photoacoustic signal. Thereafter, the whole artery was scanned at 12 wavelengths (in the spectral range 680-940 nm), to provide a map of the overall architecture of the artery.

Data processing of photoacoustic scans

In Study I, data from the photoacoustic scans were first analyzed using VisualSonics Vevo LAB 3.1.0 software, where regions of interest (ROIs) were drawn in the vessel wall (not including the lumen), subcutaneous tissue, and the skin (Figure 10). For each excitation wavelength, the PA signals from all pixels within the ROI were averaged, generating a spectrum for each ROI.

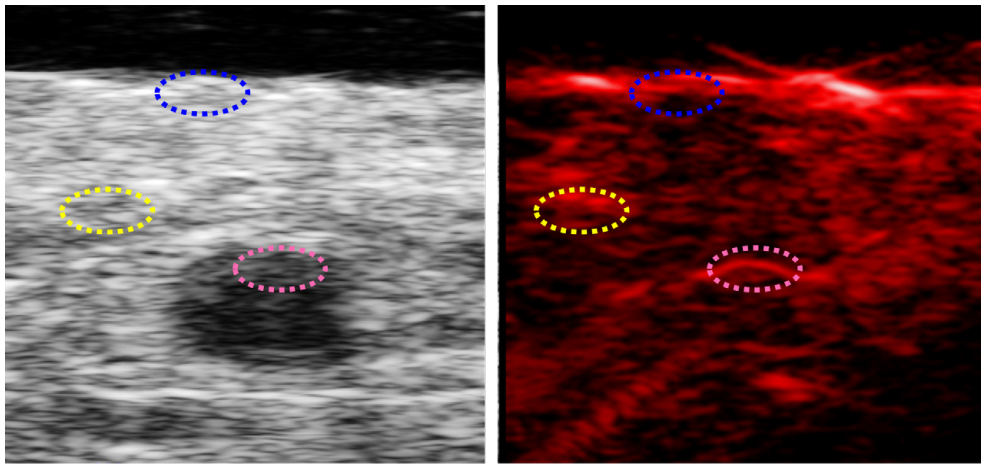

Figure 10. Representative examples of an ultrasound image (left) and a photoacoustic image (right) of a cross-section of the temporal artery. Regions of interest used for spectral analysis are shown on the artery wall (pink), the skin (blue), and the subcutaneous tissue (yellow).

The data from each measurement were then exported to MATLAB (MathWorks Inc., Natick, MA, USA) in table format for further statistical analysis. The spectra were normalized in order to allow comparison of different series of measurements. This was done using the Z-score, which scales the values of a feature so as to have a mean of 0 and a standard deviation of 1. The results of the PAI measurements are therefore expressed in arbitrary units.

In Study II, raw data from the photoacoustic scans were exported from Vevo LAB to MATLAB, where the analysis was performed. The data was first pre-processed using the ultrasound images to remove background signals, using a procedure outlined in a previous work (148). A threshold was set to differentiate the artery from the background, and the pixels belonging to the artery could therefore easily be indexed for further analysis.

Spectra were thereafter obtained by extracting the PA signal either on a pixel-by-pixel basis, as an average of a whole cross-section, or a selected ROI within a cross-section, after which spectral analysis was applied. In order to identify important spectral features and make them more visible, a spectral analysis procedure was developed and applied which decomposes the data set in order to enhance spectral contrast. For example, if we

consider the collection of pixel spectra present in a single cross-section, considering only the mean spectrum from all these pixels limits the detection of the spectral variety that could potentially be present. By decomposing the data (in this case, all the spectra obtained in the image), it is possible to identify more subtle spectral features that deviate from the mean.

The spectra were first normalized by dividing by the mean PA intensity of the entire image, in order to compare different spectra to each other. The detailed spectral analysis then involves identifying how many spectral components there are in the data set, and their relative abundance. Thereafter, each spectrum can be described based on these main spectral components and a value representing the relative abundance of each. This approach essentially captures the spectral difference in a few values, allowing for a more systematic comparison of all spectra from which spectral features can be more easily identified. This spectral analysis was performed as it is not known which chromophores would be present in the artery wall due to inflammation. The aim was thus to find *any* difference, rather than a specific difference. After the spectral analysis, the pixels were color-coded based on their spectral features to differentiate them in space.

In order to differentiate GCA-positive from GCA-negative biopsies, the spectra were clustered into five different groups based on distinct spectral features. Each cluster thus contained several spectra that are most similar to each another, meaning that the spectra in different clusters differed more from each other than spectra within the same cluster. Of these five clusters, the cluster with the most GCA-positive biopsies and the cluster with the most GCA-negative biopsies were then identified.

Further details concerning data processing and analysis are given in the relevant papers (Study I and Study II).

Statistical analysis of photoacoustic imaging

Calculations and statistical analysis were performed using GraphPad Prism version 7.0c or 9.2 (GraphPad Software Inc., San Diego, CA, USA) and MATLAB. In Study I, the Mann-Whitney test was used for comparisons of visual function before and after PAI examination using GraphPad Prism, and two-way analysis of variance (ANOVA) for repeated measures between groups using MATLAB. In Study II, an Anderson-Darling test showed normal distribution of the data using GraphPad Prism. Thereafter, the statistical difference between the spectra from the clusters with the most GCA-positive biopsies and the most GCA-negative biopsies was analyzed using two-way ANOVA with Bonferroni's multiple comparisons test for comparisons between groups (GraphPad Prism). Apart from the statistical comparison between these two clusters, the rest of the study was descriptive.

3.3 Ultrasound center frequency shift

3.3.1 The principles of ultrasound CFS

Ultrasound CFS utilizes the fact that different tissue microstructures (primarily the size of the scatterers) affect the center frequency of the backscattered pulse differently (149). The center frequency of the pulse is where the ultrasound energy is mostly concentrated.

In ultrasound CFS, an ultrasound pulse of known frequency content is transmitted into the tissue where it is reflected, and the signal is recorded by the transducer. The frequency content of the backscattered pulse will depend on the size of the scatterers in relation to the wavelength, i.e. the frequency content of the pulse. Small scatterers will return a greater proportion of higher frequencies than large scatterers. By comparing the center frequency of the transmitted ultrasound pulse to the center frequency of the backscattered pulse, and with knowledge of the transducer and pulse characteristics, the shift in center frequency can be calculated and further analyzed (Figure 11).

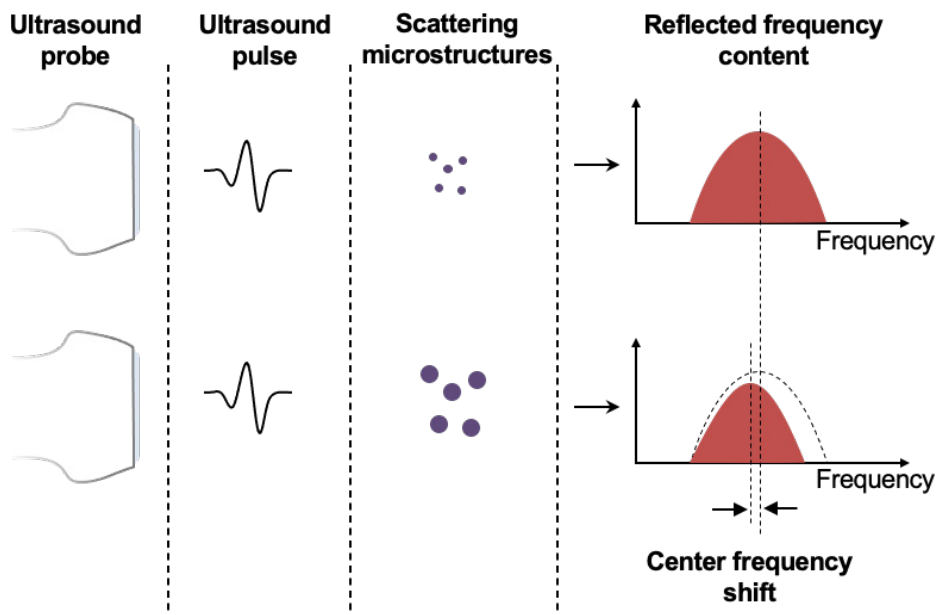

Figure 11. The principle of center frequency shift. An ultrasound pulse is transmitted into the tissue, where it is reflected. The frequency content of the backscattered pulse will depend on the size of the scatterers in relation to the frequency content of the transmitted pulse. Small scatterers will return a greater proportion of higher frequencies than large scatterers. This enables the analysis of the shift in center frequency between the transmitted and backscattered pulse, providing an objective measure of differences in tissue microstructure.

3.3.2 Ultrasound CFS equipment

In Study III, ultrasound CFS was performed using a Vevo 3100 imaging system (FUJIFILM VisualSonics Inc., Toronto, ON, Canada) equipped with a 40 MHz ultrasound linear array transducer (MX400), which has a center frequency of 30 MHz. The transducer was fixed to an adjustable arm, and the holder was driven by a stepper motor to enable 3D scanning. The same setup and ultrasound equipment were used as described in the *ex vivo* measurements with PAI (Study II), but only the ultrasound system was used in Study III and not the laser.

3.3.3 Ultrasound CFS of biopsies in cases of suspected GCA

The aim of Study III was to evaluate the feasibility of using ultrasound CFS in discriminating between biopsies assessed as positive or negative for GCA by histo-pathological examination. Patients referred for TAB were assessed for eligibility to participate in the study, and a total of 68 patients were included. After TAB, the samples were transported to a nearby laboratory for ultrasound scanning. The same setup was used as described earlier for PAI of TAB specimens (Figure 12).

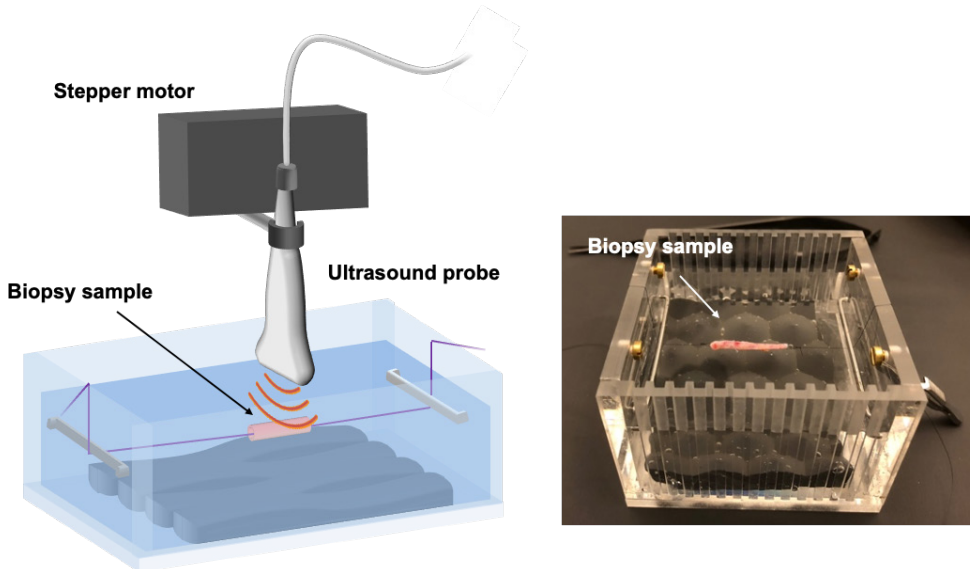

Figure 12. Illustration of the ultrasound scanning setup used to examine the temporal artery biopsy (left) and an image of the temporal artery biopsy in the container (right). The sample is mounted in a container filled with balanced saline solution. The biopsy is then scanned with an ultrasound transducer that is attached to an adjustable arm using a linear stepper motor that moves transversely with a step size of 0.5 mm.

Three-dimensional scans were obtained by moving the transducer transversely across the artery with a step size of 0.5 mm. A combined B-mode and color Doppler mode was used to obtain frequency information from two different types of ultrasound pulses, a short pulse interleaved with a long pulse. The reason for this was to reduce the impact of interference (background noise). The results were normalized to a reference, which in this case was the actual center frequency of the transducer. This was done to compensate for frequency content that is transducer dependent.

Radio frequency data were analyzed with regard to CFS using MATLAB. The tissue-related changes in the center frequency of the ultrasound signal were analyzed by comparing the frequency content of the transmitted pulse to that of the backscattered pulse. The average CFS (expressed in %) was calculated from the value for each artery in the group with positive biopsies (GCA-positive) and in the group with negative biopsies (GCA-negative). The difference in the average CFS between the GCA-positive and the GCA-negative biopsies was then determined.

After ultrasound scanning, the TAB specimens were placed in formalin and sent for histopathological examination to reveal signs of inflammation compatible with GCA. Of the 68 biopsies, 25 were positive for GCA and 43 were negative.

Statistical analysis of ultrasound CFS

Calculations and statistical analysis were performed using GraphPad Prism 9.0. The t-test was used for comparisons between groups.

3.4 Tomographic 3D ultrasound

3.4.1 The principles of tomographic 3D ultrasound

Tomographic 3D ultrasound is an electromagnetically tracked ultrasound system that enables the objective documentation of the imaged tissue and allows computerized stacks of 2D ultrasound images to be obtained through a single sweep over the target. The data from the whole examination are saved in the software, allowing for later analysis and interpretation. Tomographic 3D ultrasound images are generated using AI-based image reconstruction algorithms, allowing for the examination of vessel geometry, i.e., length, diameter, and volume (138). These 3D images of the architecture of the artery can be rotated and viewed from any angle, making the method ideal for vascular imaging due to the tortious nature of vessels.

3.4.2 Tomographic 3D ultrasound equipment

In Study IV, tomographic 3D ultrasound was performed using a Vevo MD ultra-high-frequency ultrasound system (FUJIFILM VisualSonics, Toronto, Canada) with the PIUR tUS Infinity wireless tomographic ultrasound system (PIUR imaging GmbH, Vienna, Austria), connected via an HDMI video cable. The 22 MHz and 48 MHz

transducers were used, depending on the tissue depth of the vessel. The PIUR ultrasound system consists of three components: the Infinity sensor, the Infinity video box, and the Infinity workstation. The Infinity sensor clips onto a standard ultrasound transducer and transmits the probe position in time and space via Bluetooth (Figure 13), and the Infinity video box transmits live 2D ultrasound images via Wi-Fi. The information from these two components is transmitted to the Infinity workstation.

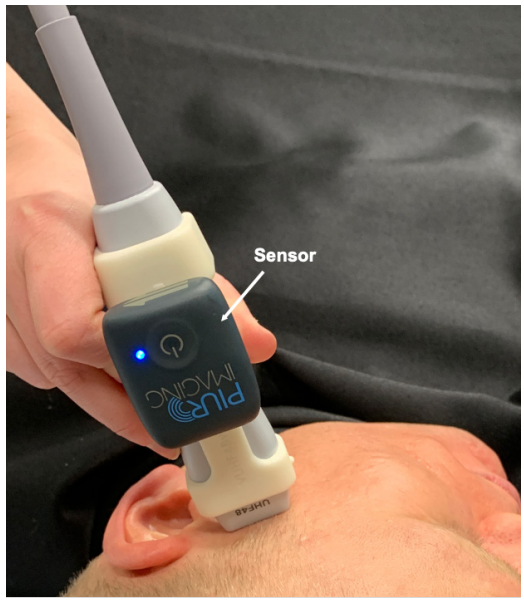

Figure 13. The sensor clips onto a standard ultrasound transducer, and conveys the transducer's position in time and space to a workstation via Bluetooth. The examination requires only a single sweep over the target tissue, and the data are stored for further analysis.

3.4.3 Tomographic 3D ultrasound investigation of healthy temporal arteries and cases of suspected GCA

The purpose of Study IV was to assess the feasibility of using tomographic 3D ultrasound to visualize the temporal artery and to measure artery dimensions. A total of 17 participants were included, 14 of which were healthy subjects, and three were patients with suspected GCA who were scheduled to undergo TAB later that day.

The superficial temporal artery was scanned in a single sweep from the level of the ear tragus following its branches (ramus frontalis and/or ramus parietalis) to as far distally as it could be visualized, with the patient supine. During the scan, a stack of live 2D images was generated, which was used to construct a 3D image of the artery in the Infinity workstation. Three to five ultrasound scans per vessel were recorded, with each scan lasting 5-10 seconds. Only the temporal artery on one side was scanned in each subject.

The complete examination took approximately five minutes for each patient. The ultrasound scanning process and postprocessing of the data are illustrated in Figure 14.

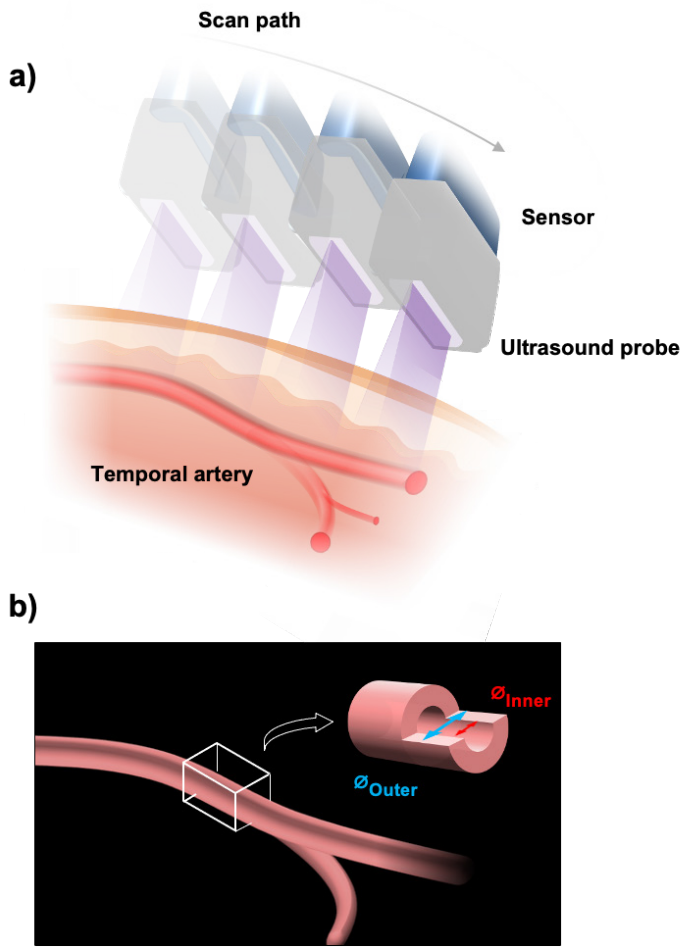

Figure 14. Scanning of the temporal artery with tomographic 3D ultrasound. a) A sensor is attached to the ultrasound transducer, which transmits information on the transducer's position in time and space during scanning. A stack of 2D images is generated, which is used for 3D reconstruction of the artery. b) This allows measurement of the inner and outer vessel diameter, to calculate the vessel wall fraction.

The scans were first processed in the PIUR software using AI-based image reconstruction algorithms, where the surrounding soft tissue was removed from the tomographic 3D image, displaying only the vessel (Figure 15). The software automatically identified the outer diameter of the vessel and the vessel length.

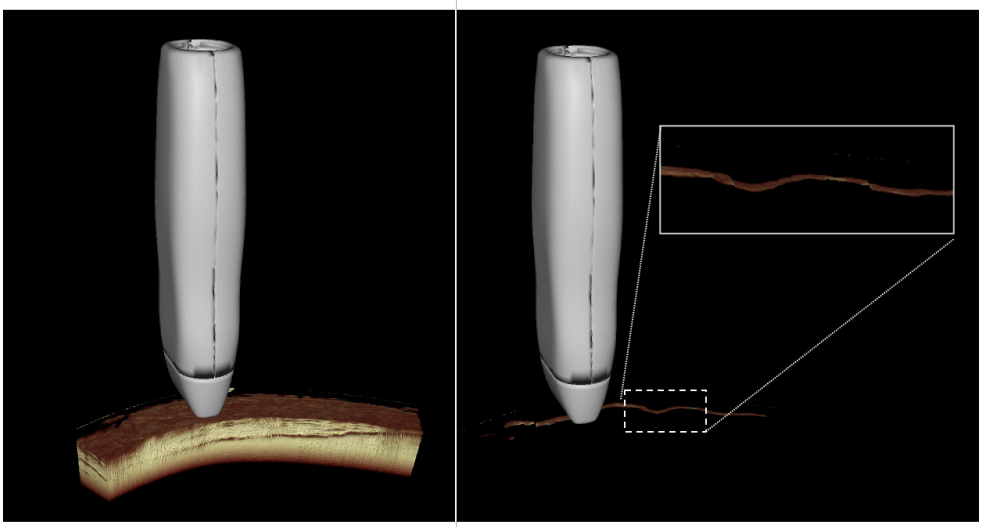

Figure 15. The surrounding tissue (left image) is removed from the image using the PIUR software, so that only the target vessel is displayed (right image).

For detailed analysis, the data were exported to MATLAB for post-processing. An algorithm was set up to display images representing cross-sectional views of the vessel, in which the user had the ability to draw lines that translate into a length. The user also had the ability to navigate through all cross-sectional images of the entire vessel and keep track of which images the lines were drawn in. To enable measurements of the inner and outer diameters of the vessel, the internal surface of the vessel (intima) and the outer border of the vessel (adventitia) were manually identified by one ultrasound examiner. Information on the characteristics of the subject was removed to enable blinded measurements. The inner and outer diameters of the artery were measured at different locations along the length of the artery, and the artery wall fraction was calculated by dividing the difference between the outer and inner diameter (obtaining the vessel wall thickness) by the outer diameter.

To examine the inter-observer agreement, the same images were assessed by another experienced ultrasound examiner, who was blinded to the measurements done by the other examiner. The obtained values of the two examiners were compared, from which Pearson correlation coefficients of 0.955 and 0.957 for the outer and inner diameters, respectively, were calculated, which suggests an excellent inter-observer agreement.

The TABs from the three subjects with suspected GCA were sent for histopathological examination, which revealed signs of GCA in one of the biopsies. The other two showed no signs of GCA and were assessed as GCA-negative.

Calculations in tomographic 3D ultrasound

Calculations were performed using MATLAB. No statistical comparisons were made between the healthy subjects and the patient with confirmed GCA due to the small sample size.

3.5 Temporal artery biopsy length

A total of 28 patients with suspected GCA undergoing TAB were included in Study V. The aim of the study was to evaluate the effect of both excision and formalin fixation on the TAB length, and to compare the results obtained from biopsies deemed to be positive and negative for GCA. TAB was performed by three different surgeons under local anesthesia, according to local practice. The biopsy length was measured *in vivo* before excision by marking the site where the artery was intended to be excised (Figure 16). When the artery was straight, the length of the intended biopsy was measured directly with a standard millimeter ruler. In cases where the artery was tortuous, surgical thread was used to trace its length, and the length of the thread was then measured to the nearest 0.5 mm. After excision, the *ex vivo* length of the biopsy specimen was measured immediately prior to formalin fixation. The specimen was then placed in 10% buffered formalin fixative and sent for histopathological examination. The length of the biopsy after formalin fixation was measured by the pathologist before sectioning for histological assessment. Patients were diagnosed as having GCA based on the histopathological findings of the biopsy, and not on the clinical presentation of symptoms. Fourteen of the biopsies were assessed as positive for GCA and 14 biopsies were negative.

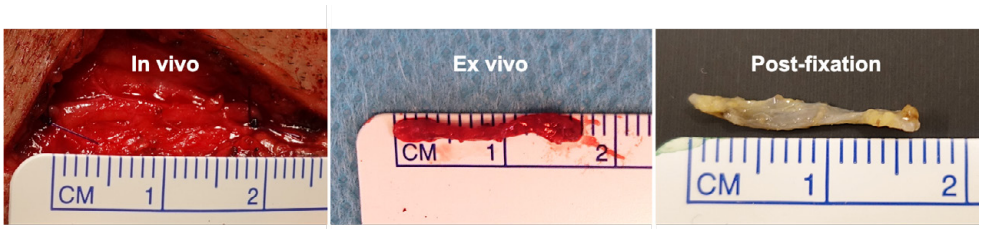

Figure 16. Measuring the temporal artery biopsy before excision (*in vivo*), after excision (*ex vivo*), and after formalin fixation (post-fixation) prior to sectioning and histopathological examination.

Statistical analysis of temporal artery biopsy length

Calculations and statistical analysis were performed using GraphPad Prism 7.0c. The Wilcoxon matched-pair test was used for paired comparisons, and the Mann-Whitney test was used for comparisons between the groups of positive and negative biopsies.

4 Results and Discussion

4.1 Photoacoustic imaging of healthy temporal arteries and safety evaluation

The feasibility of using PAI for the examination of the temporal artery and the safety of the technique were evaluated in healthy subjects in Study I. PAI did not affect the best-corrected visual acuity, color vision, or the visual field. The level of discomfort was low, and only little heat and light sensation were reported. The spectral signatures of the artery wall could be clearly differentiated from those of the surrounding tissue, and were clearly different from the subcutaneous tissue in the wavelength range 830-895 nm, and the skin in the wavelength range 795-940 nm (Figure 17). The temporal artery could be clearly delineated in the 3D scans. Thus, PAI can be used to examine the temporal artery non-invasively, *in vivo*, without the risk of affecting the visual function.

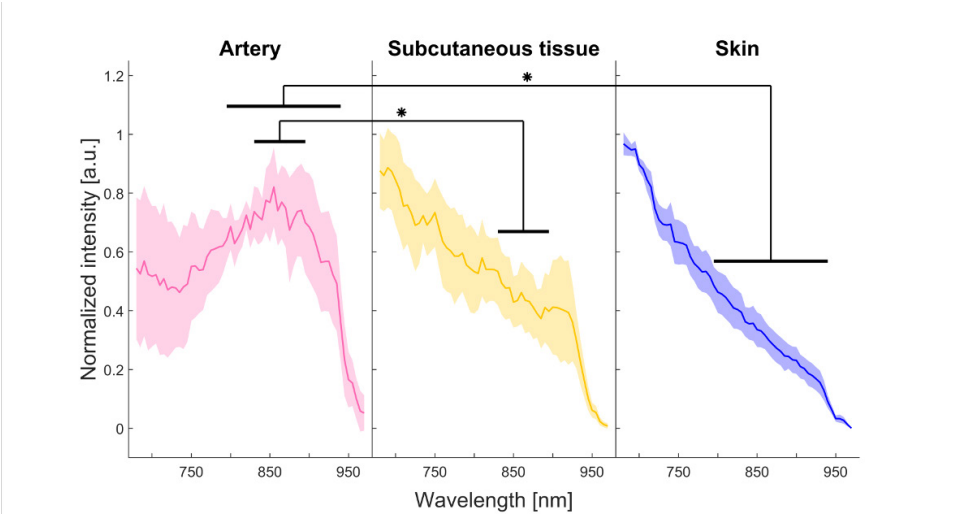

Figure 17. Photoacoustic spectra obtained from the temporal artery, the subcutaneous tissue, and the skin. The spectral signature of the artery wall was significantly different from that of the subcutaneous tissue in the wavelength range 830-895 nm, and from that of the skin in the wavelength range 795-940 nm. Significance was defined as $p<0.05$ (*).

PAI has been used previously for the visualization of other tissues and vasculature in humans (129-133, 135, 150-152), and prior to the study presented in this thesis, our research group had adapted the photoacoustic technique for examination of the temporal region in humans (136). A number of challenges associated with signal quality and resolution were addressed in that study, in order to adapt PAI to the clinical setting, and laser levels were measured. However, no detailed investigation of safety regarding visual function or patient tolerability was carried out in that previous study.

It is important to consider the safety of both patients and health care professionals when translating a technique from experimental to clinical use. Visual function of the study subjects was tested before and after PA examination, and found to be unaffected. This is an important finding as it shows that the technique may be developed as a safe diagnostic tool for GCA in the clinical setting. The reason for caution is primarily that the choroid contains pigment cells, which contain melanin, and this strongly absorbs light in the 680-970 nm wavelength range. The high absorption, together with the focusing effect of the lens and cornea, may pose a potential risk for measurements around the eye when using PAI. However, the subjects' eyes were covered with eye shields that absorb all wavelengths, and the examination was not expected to have any negative effect on visual function. The only light that might reach the eye is that which is diffusely scattered through the tissue surrounding the temporal area, but the energy levels are too low and the photons too scattered to cause any damage to the retina or the optic nerve.

An advantage of PAI is that it is less user-dependent, since the spectral signature in the vessel wall is an objective measure. The results obtained from Study I show that PAI can be used to delineate the temporal artery objectively, and that the spectral signature of the artery in healthy subjects is unique, which is the first step towards the evaluation of GCA using PAI. It could be speculated that PAI has a greater ability to detect small differences in the artery wall since the absorption spectrum depends on the molecular composition of the tissue. It can therefore be assumed that small differences in the tissue, and between healthy and diseased vessels, could be analyzed. Confirmation of this would require a larger clinical study, including both healthy and diseased vessels, together with technical improvements to compensate for noise in the data, such as that caused by movement artefacts.

Thus, it was concluded that PAI can be used for the examination of the temporal artery in human subjects in a safe and tolerable way. The artery wall was clearly delineated, and unique spectral signatures were obtained for the artery and the surrounding tissues.

4.2 Mapping the temporal artery using photoacoustic imaging

The aim of Study II was to use multispectral PAI for detailed spectral and spatial characterization of the temporal artery *ex vivo*, in biopsies classified as positive or negative for GCA. The spectral signature of temporal arteries was extracted by analyzing 259 cross-sections from 77 TAB specimens. PAI was able to map the architecture of the temporal artery, providing detailed spectral information, while the spectral analysis indicated a difference between the spectra from GCA-positive and GCA-negative biopsies.

To further explore the extent to which the PA spectra may vary spatially within the artery, each pixel was color-coded based on distinct spectral features. This was done in a cross-section and in a longitudinal section on representative examples of a GCA-positive and a GCA-negative TAB specimen. In the cross-section, the spectral features varied within the sample scan, but also between the GCA-positive and GCA-negative biopsies. This was expected considering the structure of the artery, and the differences in molecular composition due to inflammation in the GCA-positive artery (Figure 18).

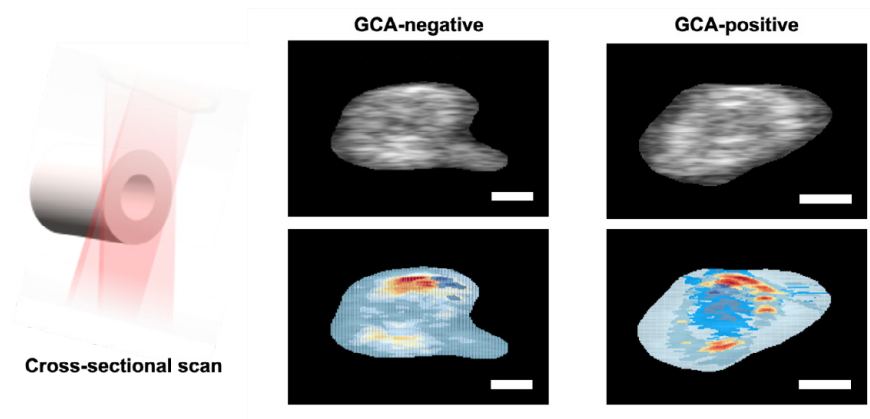

Figure 18. Cross-section of the temporal artery in GCA-negative and GCA-positive temporal artery biopsy specimens, showing the ultrasound image (top images) and the color-coded image (bottom images) based on distinct spectral features. The color scale in the images ranges from red to blue, where regions that are red differ the most spectrally from regions that are blue. The scale bars represent 1 mm.

In a longitudinal section of a positive and negative TAB specimen, a spatially resolved map of the architecture of the vessel was obtained showing different spectral features, indicating differences in the molecular composition of the artery specimen (Figure 19).

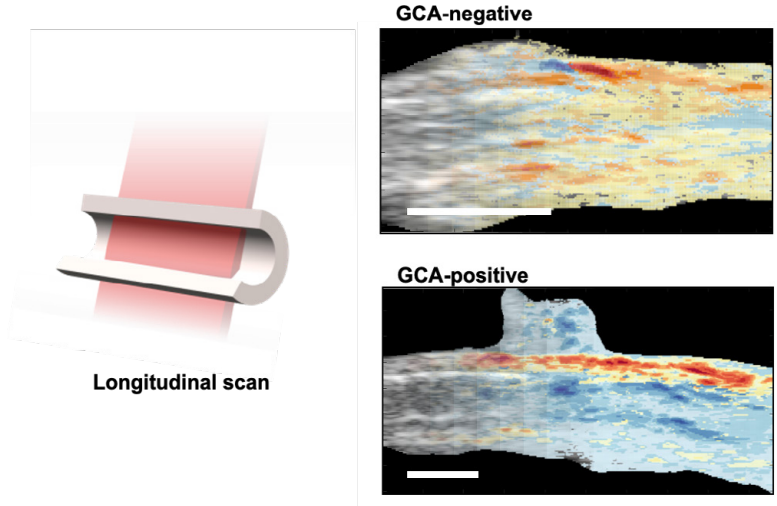

Figure 19. Longitudinal, color-coded section of temporal artery biopsy specimens from a GCA-negative and a GCA-positive sample, where each color represents a spectral feature. The color scale in the images ranges from red to blue, where regions that are red differ the most spectrally from regions that are blue. The scale bars represent 2 mm.

To obtain a more complete spectral picture of a single artery, multiple PA image stacks were acquired sequentially from different locations along the TAB specimen length of one representative GCA-positive biopsy and one GCA-negative biopsy. This showed the variability in the spectra from different locations along the length of the biopsies, which could potentially reflect the variability in the extent and distribution of the inflammation in the vessel wall seen in GCA.

By employing the spectral analysis previously described, which automatically divided all spectral features into clusters, five different clusters were identified, based on distinct spectral features. The spectral features were extracted as a spatial average over the cross-section of the artery, yielding spectra from a total of 259 cross-sections. In one cluster, which contained 27 spectra, 74% were from GCA-negative biopsies, while in another cluster, containing 83 spectra, 57% were from GCA-positive biopsies. The spectra in the cluster with the highest representation of GCA-negative biopsies were significantly different from those in the cluster predominantly comprising GCA-positive biopsies in the wavelength range 688-970 nm (except in the range 770-785 nm) ($p<0.0001$), suggesting that there are some spectral differences between GCA-negative and GCA-positive biopsies. While these findings are promising, there is a need of improvement of the technique. In its current state of development, PAI alone may not provide the reliability required for a definitive GCA diagnosis, and it will probably have to be combined with clinical parameters to ensure diagnostic accuracy.

PAI has been used previously to image human vasculature, but most of these studies have employed a limited number of excitation wavelengths, and are based on the detection of oxygenated and deoxygenated hemoglobin, which strongly absorb light of

different wavelengths, thus providing good PA contrast (128, 129, 132, 133). In GCA, the inflammation resides in the vessel wall, and measurements on the hemoglobin inside the artery are therefore not sufficient for diagnosing GCA. The results from Study II showed that PAI, in combination with advanced spectral analysis, can be used to obtain detailed spatially resolved PA spectra from temporal arteries, without *a priori* knowledge of which chromophores that may be present, and that it provides important information on the artery wall itself, which is promising for the clinical implementation of PAI. However, further technical development and methods of analysis are needed to identify the spectral signatures of arteries with GCA, and to differentiate these from healthy arteries.

The temporal arteries were examined *ex vivo*, which eliminates motion artifacts and reduces the impact of chromophores in circulating blood and in the tissue above the artery. *In vivo* spectra are therefore expected to be more challenging to analyze due to the presence of PA signals from surrounding tissue (136), which must be compensated for. However, these are not fundamental limits, but rather technical problems that can be overcome. Further studies are needed and a number of issues need to be addressed before the technique can be clinically implemented, including technical development for motion tracking and techniques to correct for spectral coloring (see Challenges and future perspectives).

4.3 Discriminating between GCA-positive and GCA-negative biopsies using ultrasound CFS

The feasibility of using ultrasound CFS for the detection of GCA in TAB specimens was investigated in Study III. The results showed that ultrasound CFS has the potential to differentiate temporal arteries with GCA from those without GCA, *ex vivo*. The mean CFS (%) decreased significantly less in biopsies positive for GCA (CFS (%) 3.83, 95% CI 3.68-3.97) than in biopsies negative for GCA (CFS (%) 4.02, 95% CI 3.90-4.13) (Figure 20).

Ultrasound CFS has previously been shown to be able to identify lesion components of vessel plaques contributing to plaque vulnerability and the risk of vascular events (137), but its feasibility for future GCA diagnosis has not been investigated until now. The main advantage of ultrasound CFS is that it is less dependent of the expertise of the examiner since the CFS value obtained is an objective measure. This is in contrast to conventional ultrasound methods based on B-mode images, such as color Doppler ultrasound, which are dependent on the operator's experience (102) and are thus prone to inter-observer variability. Ultrasound CFS can be performed with any ultrasound scanner that also has a Doppler ultrasound function, to enable the dual-pulse approach described in this study. Following a software upgrade for the analysis of CFS, the technique could become widely available at many clinics already using ultrasound. However, even though the technique could potentially be implemented easy, its application in various clinical scenarios is far from complete. The role of ultrasound

CFS in diagnosing GCA needs further evaluation concerning its diagnostic performance before its clinical applicability can be considered. The study presented in Study III only assessed whether there was a difference on a group level between GCA-positive and GCA-negative biopsies and did not evaluate the predictive utility in the diagnosis of GCA, which should be the focus of future studies.

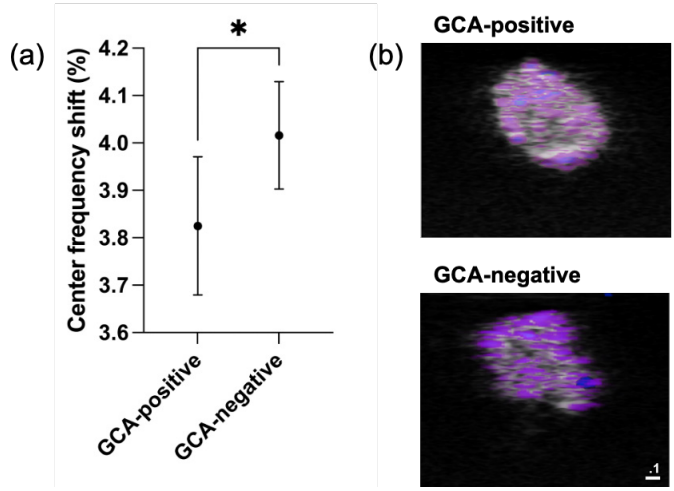

Figure 20. a) Graph showing the center frequency shift (CFS %) for GCA-positive and GCA-negative biopsies, as mean values with 95% confidence intervals. Significance was defined as $p<0.05$ (*). b) Representative examples of CFS images of biopsies that are positive and negative for GCA. The value of CFS (%) for each pixel is shown as a purple overlay. Scale bar is 0.1 mm.

One limitation of the study presented in Study III, as for many previous studies assessing GCA, is the difficulty in defining the patient inclusion criteria, since there are no established diagnostic criteria for GCA. Many previous studies have used the 1990 ACR criteria for GCA (88). However, these are classification criteria, and cannot be used to diagnose GCA in individual cases. The subjects in Study III were divided into those who were classified positive and those who were negative for GCA based on histopathological examination of the temporal artery.

This study showed that ultrasound CFS has the potential to differentiate between TAB specimens with and without histological signs of GCA. Further technical development is needed to make *in vivo* examination possible, in order to evaluate whether ultrasound CFS can be used for the diagnosis of GCA.

4.4 Visualizing the temporal artery using tomographic 3D ultrasound

Since the degree and extent of the inflammation in the vessel wall in GCA can vary, it is of benefit to examine the whole length of the accessible artery. This is possible, to some degree, using conventional 2D ultrasound, but the interpretation is highly dependent on the experience of the operator, and the diagnostic sensitivity therefore varies (97, 98, 153, 154). Tomographic 3D ultrasound can be used to map the whole architecture of the temporal artery and to measure vessel geometry, as demonstrated in Study IV. The 3D images showed that the arteries decreased in diameter distally from the level of the ear tragus, and the outer diameter of the vessel varied between the subjects depending on how distally the artery was scanned, in accordance with normal vessel anatomy (Figure 21). No distinction could therefore be made between the healthy arteries and the artery affected by GCA, based on these measurements.

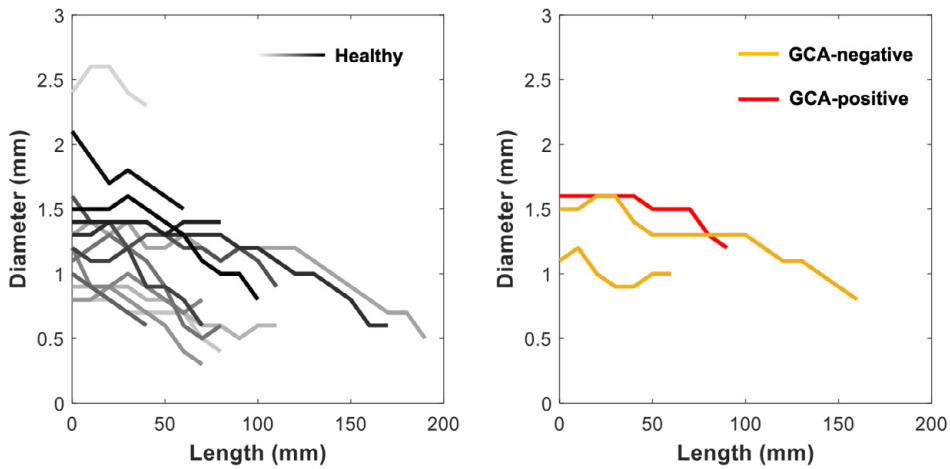

Figure 21. The length and outer diameter of the temporal artery in healthy subjects (left) and in patients with suspected giant cell arteritis (right). No differences were observed between these groups when assessing only the outer diameter.

In order to visualize the relation between the artery wall thickness and the total vessel diameter, the artery wall fraction was calculated by dividing the wall thickness by the total vessel diameter (Figure 22). The artery wall fraction for the GCA-positive patient was high, revealing the combination of vessel wall thickening and lumen narrowing, which may be indicative of GCA (Figure 23). However, no statistical analysis was performed.

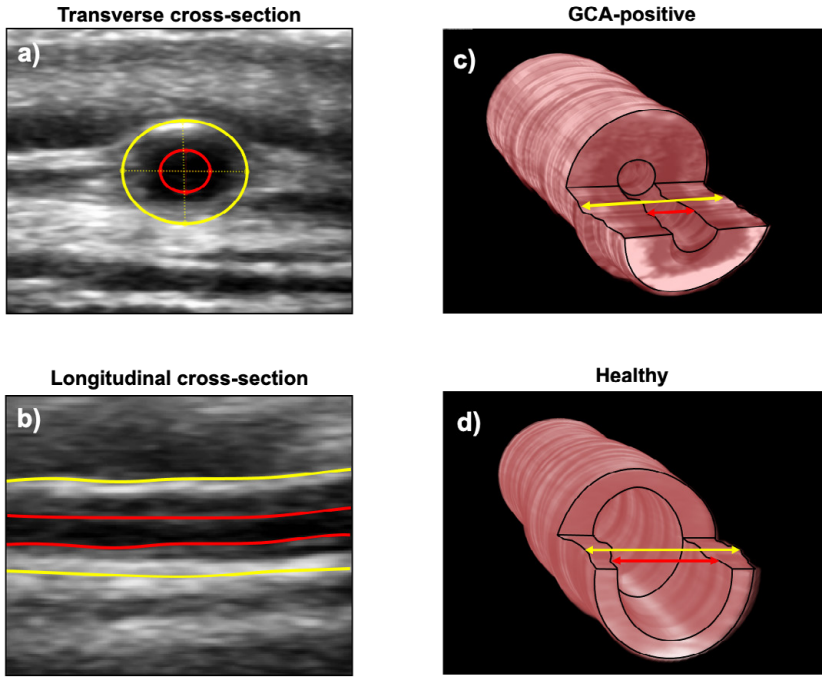

Figure 22. Detailed images showing delineation of the inner and outer artery wall of the GCA-positive artery in the transverse a) and longitudinal b) directions. 3D reconstructions of the architecture of the GCA-positive artery and a typical healthy artery are shown in c) and (d), respectively. Note the vessel wall thickening and narrowing of the lumen in the GCA-positive artery.

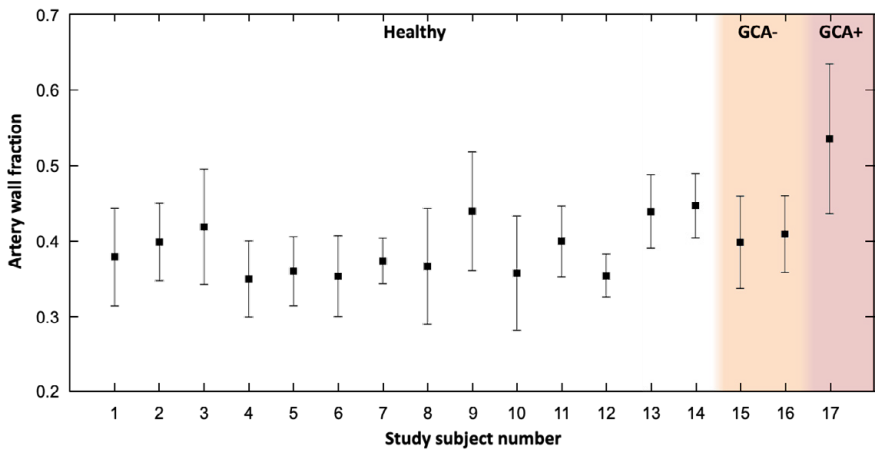

Figure 23. The artery wall fraction, calculated by dividing the vessel wall thickness (the difference between the outer and inner vessel diameter) by the outer diameter throughout the length of the vessel in each patient assessed as healthy, GCA-negative (GCA-) or GCA-positive (GCA+). Data are plotted with the mean represented as solid squares and the error bars representing +/- 1 standard deviation (SD). Note the high artery wall fraction in the GCA-positive subject.

Previous studies have shown that tomographic 3D ultrasound is useful for the mapping of other blood vessels. It can be used to measure vessel geometry, such as length, luminal diameter and vessel wall volume (138), and, for example, in assessing arterial stenosis in the lower extremities (139), carotid plaque volume (140, 155), abdominal aorta aneurysm (141), and for imaging small arteries, such as the digital arteries (156), offering several advantages over conventional 2D ultrasound. Data on the complete architecture of the artery are saved, allowing post-processing and detailed measurements of vessel dimensions from any angle (138). Furthermore, relying on artery wall measurements, instead of the halo and compression signs when examining the temporal arteries, makes the interpretation less operator-dependent.

Thus, the results of Study IV indicate that tomographic 3D ultrasound has the potential to measure vessel wall geometry over the full extent of the examined artery, and may constitute a more operator-independent diagnostic tool for GCA in the future. However, a larger study must be carried out to enable statistical comparison between healthy and GCA-positive subjects.

4.5 Clinical benefits of a future non-invasive diagnostic tool for the diagnosis of GCA

The clinical advantages of introducing a non-invasive diagnostic tool for GCA are many. Firstly, this could replace surgical biopsy, thereby avoiding the surgical risks associated with this invasive approach.

Secondly, it would allow the examination of a greater length of the temporal artery than a surgical biopsy, which is of benefit as GCA can present with skip lesions (63). Furthermore, other vessels involved in GCA, for example, the axillary artery, can be examined, thereby increasing the probability of finding inflammatory changes in the arteries. In GCA, the axillary arteries are affected in up to 50% of patients (40, 41) and TAB specimens are negative in over half of patients with extracranial GCA (41). Studies investigating both temporal and axillary arteries have revealed consistently higher sensitivities than those focusing on temporal arteries only (109). The additional diagnostic benefit of imaging the extracranial arteries in such cases is obvious. In contrast to MRI and FDG-PET/CT, these novel techniques can be used at the bedside, and are generally well tolerated by patients.

Thirdly, a non-invasive technique could potentially allow the effect of treatment to be monitored over time, which could improve the treatment of patients with GCA. The sensitivity of color Doppler imaging is significantly reduced within the first week of therapy with corticosteroids (116), but histopathological findings due to GCA are seen after a longer period microscopically than with ultrasound. Recently, the IL6-receptor inhibitor tocilizumab has become a standard part of GCA treatment. This agent interferes with the ability to generate an acute phase response, as assessed by ESR or CRP, thereby lessening the influence of these biomarkers on the clinical assessment of

disease activity in GCA. Imaging modalities therefore may contribute to a more comprehensive assessment of patients with GCA. Follow-up studies must be carried out to investigate whether PAI, ultrasound CFS, or tomographic 3D ultrasound can be used to detect the subtle differences due to inflammation when treatment has been initiated with corticosteroids or other immunomodulatory drugs.

4.6 The effect of excision and formalin fixation on temporal artery biopsy length

The accuracy of the histopathological diagnosis of GCA is believed to be correlated to the length of the formalin-fixated artery specimen that is available for histopathological examination (74, 87). The biopsy may shrink following excision and formalin fixation, which is of clinical importance since the biopsy length is determined before excision. The results obtained in Study V show that the TAB contracts upon surgical excision, but no further shrinkage was seen following formalin fixation (Figure 24). The median contraction upon surgical excision was 12% for the negative biopsies and 15% for the positive biopsies, but the difference was not statistically different between these groups. The surgeon can therefore be confident that the length of the biopsy measured after excision is the actual length analyzed histopathologically.

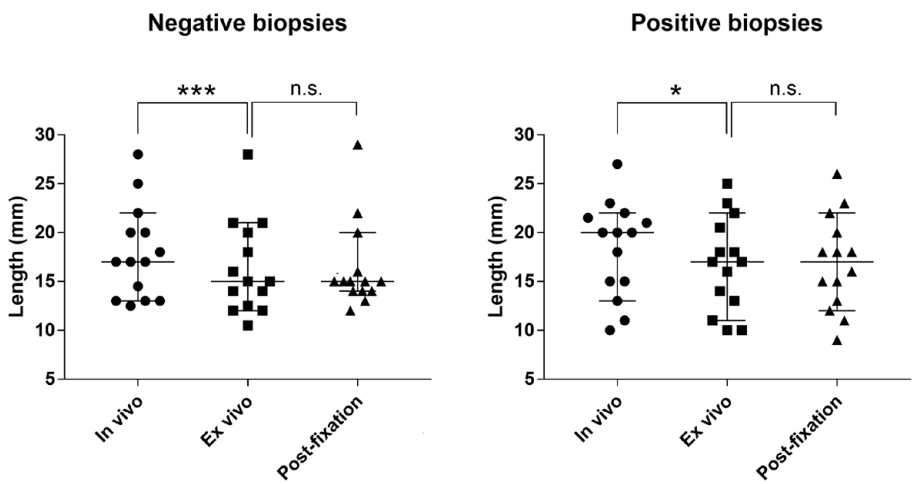

Figure 24. The length of the temporal artery biopsy specimens before excision (*in vivo*), directly after excision (*ex vivo*) and after formalin fixation (post-fixation) in biopsies negative (left) and positive (right) for giant cell arteritis according to histopathological findings. Significance was defined as $p<0.05$ (*), $p<0.01$ (**) and $p<0.001$ (***); n.s, not significant.

No previous studies have been carried out to determine the length of temporal artery biopsies before excision, directly after excision, and after formalin fixation. In a study by Su et al., the length of the temporal artery biopsy was measured before and after excision, showing a mean contraction of 20% (80). The effect of formalin fixative on TAB length has been evaluated in other studies, in which a shrinkage of 8-15% was reported (84-86). This is in contrast to our findings of no shrinkage after formalin fixation.

The difference in shrinkage between positive and negative biopsies was also investigated. It has previously been reported that the contraction of TAB specimens after surgical excision was less in biopsies assessed as positive for GCA than in negative biopsies, but the number of positive biopsies was low relative to the GCA-negative biopsies in that study (80). It has also been found in previous studies that there is a correlation between systemic inflammation and reduced arterial elasticity in vasculitis in other parts of the body (78, 79). Since it has been reported that the biopsy length is generally longer in positive TABs (72-75), this raises the question of whether the difference in length between positive and negative TABs is due to greater contraction of the negative specimens rather than the diagnostic accuracy of the length. In Study V, no statistically significant difference was seen in shrinkage between positive and negative TAB specimens, which is in agreement with the findings of a recently published study on the effect of formalin fixation (86).

A limitation of the present study was that the length of the TAB specimens was measured by three different surgeons and pathologists, which may have introduced interindividual variability in the measurements.

Further studies are needed on the effect of both surgical excision and post-surgical processing for histopathological examination, in which the measurements are made by the same surgeon and pathologist, to confirm that shrinkage does not affect TAB length to a degree that affects the diagnostic accuracy. Regardless of any recommended length, longer specimens are only valuable if additional histologic sections are examined, emphasizing the need for standardized protocols in both studies and clinics.

5 Conclusions

The conclusions drawn from the studies presented in this thesis can be summarized as follows.

- PAI of the temporal artery is well tolerated and safe with regard to visual function. The spectral signature of the healthy temporal artery is unique, and the artery can be clearly differentiated from the surrounding tissue.
- PAI can be used to map the architecture of the temporal artery *ex vivo*, providing detailed spectral and spatial information. The spectral analysis indicated a difference between the spectra from GCA-positive and GCA-negative biopsies.
- Ultrasound CFS has the potential to differentiate temporal arteries with GCA from those without GCA *ex vivo*.
- Tomographic 3D ultrasound can be used to visualize the temporal artery and to measure geometric features of the vessel, such as the vessel wall fraction.
- TAB specimens contract upon surgical excision, and the difference in contraction between specimens assessed as positive and negative for GCA was not statistically significant. No further contraction was seen as a result of formalin fixation.

5.1 Challenges and future perspectives

Improvements must be made before PAI, ultrasound CFS, or tomographic 3D ultrasound can be used as non-invasive, diagnostic tools for GCA, either as substitutes for or in conjunction with histopathological examination.

Before achieving precise *in vivo* imaging and analysis of the temporal artery with PAI, it is essential to develop fluence compensation techniques. The optical fluence (energy deposition) is not uniform within the tissue and the effects of absorbing chromophores in the circulating blood and in tissue above the artery give rise to spectral coloring, which is a phenomenon that occurs as photons travel deeper into the tissue and undergo wavelength-dependent absorption in different tissue layers (157). The arterial depth, and the concentration of different chromophores such as melanin and hemoglobin (and its

oxygenation status) will affect the fluence spectrum reaching the artery and may affect the results. Furthermore, the intraluminal signal from hemoglobin when imaging blood vessels will lead to spectral absorption that is considerably higher than that from the actual vessel wall, making it difficult to discriminate the spectrum of the healthy artery from that originating from inflammatory processes due to GCA. Thus, the effects of other chromophores in the tissue must be taken into consideration and techniques for post-processing of the measured data may be important in this context (158, 159).

Moreover, the implementation of motion correction techniques could contribute to enhanced image resolution. Motion artefacts arising from movements of the patient, breathing, and heart beating contribute to noise in the data. The problem of motion artefacts could be solved by the application of software to correct for motion artefacts in the image, or the use of electrocardiography to trigger image capture to compensate for arterial pulsation. Methods based on machine-learning for motion corrected PA images may be useful (160). After technical development, the next step in evaluating PAI as a clinical diagnostic tool for GCA involves conducting studies on *in vivo* examinations of temporal arteries.

The ultrasound CFS technique must also be further refined and this can be achieved by the implementation of methods aimed at improving the estimation of the frequency shift. The dual-pulse approach used in Study III, in order to remove the background signal that is not related to tissue microstructure, constitutes a potential limitation of ultrasound CFS, as this may lead to an error in the estimated CFS. Tuning the pulse parameters could improve this method, and this is discussed in more detail in Study III. Furthermore, the frequency attenuation in tissue above the artery will affect the estimated CFS and must be compensated for, together with the effects of movement artefacts. Following these improvements, validation studies are required to assess the diagnostic performance of ultrasound CFS in GCA, before it can be considered as a clinical diagnostic technique for GCA.

To enhance the 3D reconstructions obtained with tomographic 3D ultrasound, the data from the B-mode ultrasound must be further optimized. The analysis in tomographic 3D ultrasound relies on the data from the B-mode ultrasound, which means that any error present in the B-mode image will be translated into the 3D reconstruction and the following measurements. This also applies to artefacts that degrade the resolution in B-mode ultrasound, which limits the 2D images to be reconstructed to 3D images. The fact that the inner and outer vessel border must be manually defined is also a source of operator-dependent error, and is time consuming. Future development, including optimization of the B-mode ultrasound, and automatic vessel border detection using AI, would thus be of great benefit.

In future applications, the efficacy of employing PAI, ultrasound CFS, and tomographic 3D ultrasound for the diagnosis of GCA is likely to be enhanced through the integration of the results from these techniques, given that each method provides distinct information. PAI, for instance, may facilitate discrimination between healthy vessels and those with inflammation by examining the molecular composition of the tissue and the associated spectral signatures. Ultrasound CFS, on the other hand, enables

differentiation based on the size of the microstructures within the tissue, potentially distinguishing vessels with inflammation from those without. Additionally, tomographic 3D ultrasound provides comprehensive 3D images of the vessel anatomy and dimensions, facilitating macroscopic evaluation. The sensitivity and specificity of any non-invasive diagnostic tool for the diagnosis of GCA will probably be improved when combined with clinical predictor variables obtained from the examination of patients with suspected GCA. Since the spectral signature from the vessel wall obtained with PAI and the CFS value obtained with ultrasound CFS are both objective measures, they could potentially be used in prediction models based on the machine-learning techniques for the diagnosis of GCA.

In conclusion, a non-invasive diagnostic tool that can replace the invasive TAB approach with its surgical risks and low diagnostic sensitivity would be of great benefit to patients, healthcare professionals, and society. Timely and reliable diagnosis of GCA would enable the early initiation of treatment, thereby preventing the vascular complications associated with GCA, while at the same time avoiding the unnecessary treatment of patients who do not have GCA. The results presented in this thesis are an important step towards enabling non-invasive diagnosis of GCA. The next step in the development of PAI, ultrasound CFS, or tomographic 3D ultrasound into a clinical diagnostic tool will require technical improvements and large clinical trials in which patients suspected of having GCA are examined before undergoing surgical biopsy and compared to healthy subjects. Hopefully, this will enable the non-invasive diagnosis of GCA.

Acknowledgements

Stort tack till alla som har bidragit till min avhandling och till livet i stort! Ett särskilt tack till er som nämns här nedan. Ert stöd har varit ovärderligt.

…

Malin Malmsjö, professor och huvudhandledare, som lever och lär enligt mottot att allt går, vilket har blivit lite av en övertygelse i vår forskningsgrupp. Inspirerar i allt hon gör och ger oss vingar att flyga högre, med en lika stark hängivenhet i varje steg på vägen. Det är ett sant privilegium att forska med dig och du är en sådan handledare som jag önskar att alla doktorander kunde få uppleva. Du är en klippa!

Rafi Sheikh, min bihandledare och kollega, som från första dagen på jobbet tog mig under sina vingar. Otroligt smart och visar alltid ett stort engagemang. Levererar pepp med brutal ärlighet på den skönaste dialekten. Tack för att du trodde på min potential, för ditt ständiga stöd och för att du gjorde det möjligt för mig att börja forska.

Björn Hammar, min bihandledare, kollega och ankare på jobbet. En legend inom neurooftalmologin med en passion för ämnet som inspirerar. Ställer alltid upp, stöttar och delar med sig av nyfunnen kunskap. Jag är så tacksam för din eviga uppmuntran och för att du gör vårt jobb till världens bästa!

…

Ulf Dahlstrand, en otroligt klipsk och skicklig kollega. Besitter så många goda egenskaper, där den i särdeles bästa är hans humor. Missar inte ett kommatecken. Trodde jag. Tills vi fick John i forskningsgruppen.

Aboma Merdasa, ingenjör och stjärna i forskningsgruppen som tillför ljus, på så många sätt. En fena på att göra fina illustrationer (som samtliga i min kappa) och på att baka kanelbullar. Jag är så tacksam för all din hjälp med min forskning och mer därtill. Det hade inte varit detsamma utan dig.

Kajsa Tenland, kollega och ”Ögontös”, som jag delar de trevligaste kaffestunderna med. Besitter ett så mjukt och varmt sätt som hänför oss alla (och i synnerhet patienter <18 år). Tack för allt stöd inför slutförandet av min avhandling!

John Albinsson, ingenjör i gruppen som gör ultraljud till synes lätt och begripligt. Alltid vänlig, alltid hjälpsam och med ett smittsamt glatt humör.

Johanna Vennström Berggren, kollega och vän som alltid är villig att hjälpa. Svarar utan minsta tvekan ”javisst!” om man ber om en tjänst (innan hon ens vet vad det rör sig om). Så mild i sitt sätt och har en fantastisk förmåga att minnas de personliga detaljerna om var och en av oss.

Karl Engelsberg, kollega som bemöter alla på ett exemplariskt vänligt sätt och är lika gemytlig som en varm kopp te.

Josefine Bunke, doktorandkollega från Växjö, som alltid bjuder in till trevliga pratstunder och är så oerhört lätt att tycka om.

Linn Engqvist, fashionistan i gruppen, som är så härligt entusiastisk, positiv och effektiv. Jag kan redan nu se hur hon blir en stilsäker och käck pantertant, medan vi andra fortsätter gå i våra slitna tofflor.

Bodil Gesslein, skicklig forskarkollega och oljan i maskineriet som gör allt det administrativa så mycket lättare för oss alla. Tack!

Magnus Cinthio och **Tobias Erlöv**, ingenjörer på LTH som bidrar med ovärderliga ultraljudskunskaper för en (f.d.) teknisk analfabet som mig.

Sofia Paulsson, doktorandkollega från Jönköping, som jag har fått förmånen att jobba nära. Väldigt driven, noggrann och alltid vänlig. Jag ser så fram emot alla spännande projekt som väntar oss!

Olof Neumann, forskarkollega som tillhör de bästa i bygget på att programmera. Är lika svag för choklad som jag är.

Cu Dybelius Ansson, empatisk och alltid välklädd kollega som är som en varm kram. Genomgod ända in i märgen och artig som få. Är just nu ute på nya äventyr, men jag hoppas att vi får jobba tillsammans igen, på ett sätt eller ett annat.

Jenny Hulth, kollega som alltid är villig att hjälpa och gör det dessutom på ett ständigt trevligt sätt. Besitter ett tålamod som få.

Ett stort tack även till resten av min fantastiska forskningsgrupp, gamla som nya medlemmar! **Magne Stridh, Jens Nääv Ottosson, Hanna-Maria Öhnell** och **Khashayar Memarzadeh**– för den roliga, familjära och kreativa miljön som var och en bidrar till och som har kommit att kännetecknа vår grupp.

…

Jonas Blohmé, legend på vår klinik (och utanför!) med ett stort hjärta. Tillför så mycket på så många sätt. Korridorerna hade ekat tomma utan dig!

Pegah Torabi och **Elin Björk Tryggvadóttir**, mina allierade i neurooftalmologiteamet som alltid ställer upp. Tack för ert tålamod och förståelse inför slutförandet av min avhandling. Jag hade inte kunnat önska mig bättre kollegor.

Monika Meinert, en minst sagt härlig kollega, som är varm och sprudlande - som en strålande sol! Tack för alla roliga pratstunder och för all uppmuntran genom åren.

Stellan Molander, min kaffekompis på jobbet som jag delar de mest underhållande samtalen med. Skicklig och jobbar hårt, samtidigt som han är sådär beundransvärt chill.

Mina töser på ögonkliniken, **Ellen Sönnergren Blomsterberg, Carmen Scurei** och **Tove Faxén.** Ni är sociala som få, med skinn på näsan och så oerhört roliga att ha i sin närvaro.

Mina kollegor från Helsingborgstiden, **Johan Ursberg** och **Anna Åberg**. För ert stöd när jag behövde det som mest. Till **Marcus von Knorring**, som tog vid när jag kom till Lund och som nu dessutom ger mig möjlighet att utveckla mina pedagogiska färdigheter.

Uzma Chaudhry, kollega och vän sedan tiden på medicinkliniken i Helsingborg. Lunchkompis deluxe som boostar mig i allt mellan himmel och jord.

Vesna Ponjavic, för ditt outtröttliga engagemang för oss alla under tiden som ST-läkare. Dina skor kommer att vara svåra att fylla när du går i pension till hösten.

Ola Rauer, för din ständigt utsträckta hand när vi behöver hjälp med kluriga patientfall.

Klinikledningen **Eva Kretz, Joakim Thylefors, Carin Gustavsson,** och **Anette Lindström.** Tack för ert fantastiska arbete med att göra vår arbetsplats till den bästa och för att ni uppmuntrar till och möjliggör forskning. Ett särskilt tack till **Lena Rung**, som trodde på mig och lät mig uppfylla min dröm att bli ögonläkare. Du är en sann förebild för oss alla.

Alla i neurooftalmologiteamet med **Eva Hallbäck, Maria Nilsson, Annika Ahlman, Johanna Henriksson** och **Veronica Jönsson** i spetsen. För ert inspirerande engagemang i allt ni gör och för att ni bidrar till att göra det roligt att komma till jobbet varje dag!

Christina Rosdahl, Marie-Louise Brovall-Johnsson, Pernilla Olsson och övriga sekreterare. Tack för all hjälp med att agera spindeln i nätet, organisera, styra om och styra rätt.

Eva och **Sussie** på avd 40. Ni är omsorg och värme i ett paket.

Helen Sheppard, en guru inom språkgranskningen vars knivskarpa kommentarer ensamt är en motivation till att producera fler artiklar för henne att språkgranska.

Mina övriga **kollegor** på Ögonkliniken SUS. Jag hade kunnat nämna var och en av er, men risken är att dessa sidor hade blivit längre än själva kappan. Tack för era lärdomar genom åren!

…

Mina vänner, för att ni har gett mig mina bästa minnen.

Anahita Attaran, som är så mycket mer därtill. För din lojalitet och ditt orubbliga stöd. För alla våra minnen och allt det som skall komma. Tack för allt, khahare azizam.

Min stora härliga släkt. För er kärlek, uppfostran och allt det fina vi har upplevt tillsammans. Det har varit en ynnest att växa upp med er vid min sida och att träffa er är än idag bland det värdefullaste för mig.

Mormor **Vanica**, som var definitionen av styrka (i ett litet paket). Jag saknar dig så.

Min syster **Daniela**, som motiverade mig för många år sedan med orden ”per aspera ad astra” – genom svårigheter mot stjärnorna. Förstår, när ingen annan gör det. Jag är så tacksam över att ha dig, cece.

Min systerdotter **Bianca**. Du är en stigande stjärna som kan bli precis vad du vill!

Min älskade **Goce**. Tack för ditt tålamod, din kärlek och för att du alltid stöttar mig i allt som jag tar mig an. Livet är så mycket roligare med dig och du skänker mig all världens lycka. Vad hade jag gjort utan dig?

Mina söner och ögonstenar, **Filip** och **Nicholas**. Ni är kärlek som jag aldrig känt den förut. Jag älskar er oändligt och är så stolt över er!

Min pappa **Mendo**, som ställer upp alla dagar i veckan, alla tider på dygnet, oavsett vad. Vår alltiallo som fixar det som vi behöver hjälp med - redan igår. Tack för den trygghet som du har förmedlat och för att vi alltid har kunnat förlita oss på dig.

Min mamma **Nada**, som har hållit min hand genom livet. Det finns inga ord som med rättvisa kan beskriva dig. Du är hjärtat i vår familj och jag är så tacksam för dig. Jag älskar dig så, mamma.

References

1. Rahman W, Rahman FZ. Giant cell (temporal) arteritis: an overview and update. Surv Ophthalmol. 2005;50(5):415-28.
2. Saleh M, Turesson C, Englund M, Merkel PA, Mohammad AJ. Visual Complications in Patients with Biopsy-proven Giant Cell Arteritis: A Population-based Study. J Rheumatol. 2016;43(8):1559-65.
3. Dejaco C, Duftner C, Buttgereit F, Matteson EL, Dasgupta B. The spectrum of giant cell arteritis and polymyalgia rheumatica: revisiting the concept of the disease. Rheumatology (Oxford). 2017;56(4):506-15.
4. Gonzalez-Gay MA, Garcia-Porrua C, Llorca J, Gonzalez-Louzao C, Rodriguez-Ledo P. Biopsy-negative giant cell arteritis: clinical spectrum and predictive factors for positive temporal artery biopsy. Semin Arthritis Rheum. 2001;30(4):249-56.
5. Breuer GS, Nesher R, Nesher G. Negative temporal artery biopsies: eventual diagnoses and features of patients with biopsy-negative giant cell arteritis compared to patients without arteritis. Clin Exp Rheumatol. 2008;26(6):1103-6.
6. Grossman C, Ben-Zvi I, Barshack I, Bornstein G. Association between specimen length and diagnostic yield of temporal artery biopsy. Scand J Rheumatol. 2017;46(3):222-5.
7. Luqmani R, Lee E, Singh S, Gillett M, Schmidt WA, Bradburn M, et al. The Role of Ultrasound Compared to Biopsy of Temporal Arteries in the Diagnosis and Treatment of Giant Cell Arteritis (TABUL): a diagnostic accuracy and cost-effectiveness study. Health Technol Assess. 2016;20(90):1-238.
8. Borchers AT, Gershwin ME. Giant cell arteritis: a review of classification, pathophysiology, geoepidemiology and treatment. Autoimmun Rev. 2012;11(6-7):A544-54.
9. Gunawardene AR, Chant H. Facial nerve injury during temporal artery biopsy. Ann R Coll Surg Engl. 2014;96(4):257-60.
10. Smith JH, Swanson JW. Giant cell arteritis. Headache. 2014;54(8):1273-89.
11. Tucker WD, Arora Y, Mahajan K. Anatomy, Blood Vessels. StatPearls. Treasure Island (FL).2023.
12. Stenmark KR, Yeager ME, El Kasmi KC, Nozik-Grayck E, Gerasimovskaya EV, Li M, et al. The adventitia: essential regulator of vascular wall structure and function. Annu Rev Physiol. 2013;75:23-47.

13. Yonenaga K, Tohnai I, Mitsudo K, Mori Y, Saijo H, Iwai T, et al. Anatomical study of the external carotid artery and its branches for administration of superselective intra-arterial chemotherapy via the superficial temporal artery. Int J Clin Oncol. 2011;16(6):654-9.
14. Koziej M, Trybus M, Holda M, Wnuk J, Polak J, Brzegowy P, et al. The Superficial Temporal Artery: Anatomical Map for Facial Reconstruction and Aesthetic Procedures. Aesthet Surg J. 2019;39(8):815-23.
15. Meybodi AT, Lawton MT, El-Sayed I, Davies J, Tabani H, Feng X, et al. The Infrazygomatic Segment of the Superficial Temporal Artery: Anatomy and Technique for Harvesting a Better Interposition Graft. Oper Neurosurg (Hagerstown). 2017;13(4):517-21.
16. Pinar YA, Govsa F. Anatomy of the superficial temporal artery and its branches: its importance for surgery. Surg Radiol Anat. 2006;28(3):248-53.
17. Marano SR, Fischer DW, Gaines C, Sonntag VK. Anatomical study of the superficial temporal artery. Neurosurgery. 1985;16(6):786-90.
18. Medved F, Manoli T, Medesan R, Janghorban Esfahani B, Stahl S, Schaller HE, et al. In vivo analysis of the vascular pattern of the superficial temporal artery based on digital subtraction angiography. Microsurgery. 2015;35(5):380-6.
19. Jennette JC, Falk RJ, Bacon PA, Basu N, Cid MC, Ferrario F, et al. 2012 revised International Chapel Hill Consensus Conference Nomenclature of Vasculitides. Arthritis Rheum. 2013;65(1):1-11.
20. Boes CJ. Bayard Horton's clinicopathological description of giant cell (temporal) arteritis. Cephalalgia. 2007;27(1):68-75.
21. Huston KA, Hunder GG, Lie JT, Kennedy RH, Elveback LR. Temporal arteritis: a 25-year epidemiologic, clinical, and pathologic study. Ann Intern Med. 1978;88(2):162-7.
22. Stamatis P, Turkiewicz A, Englund M, Turesson C, Mohammad AJ. Epidemiology of biopsy-confirmed giant cell arteritis in southern Sweden-an update on incidence and first prevalence estimate. Rheumatology (Oxford). 2021;61(1):146-53.
23. Ponte C, Grayson PC, Robson JC, Suppiah R, Gribbons KB, Judge A, et al. 2022 American College of Rheumatology/EULAR classification criteria for giant cell arteritis. Ann Rheum Dis. 2022;81(12):1647-53.
24. Salvarani C, Gabriel SE, O'Fallon WM, Hunder GG. The incidence of giant cell arteritis in Olmsted County, Minnesota: apparent fluctuations in a cyclic pattern. Ann Intern Med. 1995;123(3):192-4.
25. Mohammad AJ, Nilsson JA, Jacobsson LT, Merkel PA, Turesson C. Incidence and mortality rates of biopsy-proven giant cell arteritis in southern Sweden. Ann Rheum Dis. 2015;74(6):993-7.
26. Sharma A, Mohammad AJ, Turesson C. Incidence and prevalence of giant cell arteritis and polymyalgia rheumatica: A systematic literature review. Semin Arthritis Rheum. 2020;50(5):1040-8.

27. Watts RA, Hatemi G, Burns JC, Mohammad AJ. Global epidemiology of vasculitis. Nat Rev Rheumatol. 2022;18(1):22-34.
28. Li KJ, Semenov D, Turk M, Pope J. A meta-analysis of the epidemiology of giant cell arteritis across time and space. Arthritis Res Ther. 2021;23(1):82.
29. Mackie SL, Taylor JC, Haroon-Rashid L, Martin S, Dasgupta B, Gough A, et al. Association of HLA-DRB1 amino acid residues with giant cell arteritis: genetic association study, meta-analysis and geo-epidemiological investigation. Arthritis Res Ther. 2015;17(1):195.
30. Carmona FD, Mackie SL, Martin JE, Taylor JC, Vaglio A, Eyre S, et al. A large-scale genetic analysis reveals a strong contribution of the HLA class II region to giant cell arteritis susceptibility. Am J Hum Genet. 2015;96(4):565-80.
31. Weyand CM, Goronzy JJ. Immune mechanisms in medium and large-vessel vasculitis. Nat Rev Rheumatol. 2013;9(12):731-40.
32. Stamatis P, Turesson C, Michailidou D, Mohammad AJ. Pathogenesis of giant cell arteritis with focus on cellular populations. Front Med (Lausanne). 2022;9:1058600.
33. Weyand CM, Goronzy JJ. Immunology of Giant Cell Arteritis. Circ Res. 2023;132(2):238-50.
34. Cavazza A, Muratore F, Boiardi L, Restuccia G, Pipitone N, Pazzola G, et al. Inflamed temporal artery: histologic findings in 354 biopsies, with clinical correlations. Am J Surg Pathol. 2014;38(10):1360-70.
35. Klein RG, Hunder GG, Stanson AW, Sheps SG. Large artery involvement in giant cell (temporal) arteritis. Ann Intern Med. 1975;83(6):806-12.
36. Wilkinson IM, Russell RW. Arteries of the head and neck in giant cell arteritis. A pathological study to show the pattern of arterial involvement. Arch Neurol. 1972;27(5):378-91.
37. Buttgereit F, Dejaco C, Matteson EL, Dasgupta B. Polymyalgia Rheumatica and Giant Cell Arteritis: A Systematic Review. JAMA. 2016;315(22):2442-58.
38. Grayson PC, Maksimowicz-McKinnon K, Clark TM, Tomasson G, Cuthbertson D, Carette S, et al. Distribution of arterial lesions in Takayasu's arteritis and giant cell arteritis. Ann Rheum Dis. 2012;71(8):1329-34.
39. Naderi N, Mohammad AJ, Turesson C. Large vessel involvement in biopsy-proven giant cell arteritis: incidence, distribution, and predictors. Scand J Rheumatol. 2017;46(3):215-21.
40. Schmidt WA, Seifert A, Gromnica-Ihle E, Krause A, Natusch A. Ultrasound of proximal upper extremity arteries to increase the diagnostic yield in large-vessel giant cell arteritis. Rheumatology (Oxford). 2008;47(1):96-101.
41. Czihal M, Zanker S, Rademacher A, Tato F, Kuhlencordt PJ, Schulze-Koops H, et al. Sonographic and clinical pattern of extracranial and cranial giant cell arteritis. Scand J Rheumatol. 2012;41(3):231-6.
42. Bley TA, Weiben O, Uhl M, Vaith P, Schmidt D, Warnatz K, et al. Assessment of the cranial involvement pattern of giant cell arteritis with 3T magnetic resonance imaging. Arthritis Rheum. 2005;52(8):2470-7.

43. Smetana GW, Shmerling RH. Does this patient have temporal arteritis? JAMA. 2002;287(1):92-101.
44. Martinez-Taboada VM, Alvarez L, RuizSoto M, Marin-Vidalled MJ, Lopez-Hoyos M. Giant cell arteritis and polymyalgia rheumatica: role of cytokines in the pathogenesis and implications for treatment. Cytokine. 2008;44(2):207-20.
45. Healey LA, Wilske KR. Presentation of occult giant cell arteritis. Arthritis Rheum. 1980;23(6):641-3.
46. Gonzalez-Gay MA, Lopez-Diaz MJ, Barros S, Garcia-Porrua C, Sanchez-Andrade A, Paz-Carreira J, et al. Giant cell arteritis: laboratory tests at the time of diagnosis in a series of 240 patients. Medicine (Baltimore). 2005;84(5):277-90.
47. Gonzalez-Gay MA, Garcia-Porrua C, Llorca J, Hajeer AH, Branas F, Dababneh A, et al. Visual manifestations of giant cell arteritis. Trends and clinical spectrum in 161 patients. Medicine (Baltimore). 2000;79(5):283-92.
48. Aiello PD, Trautmann JC, McPhee TJ, Kunselman AR, Hunder GG. Visual prognosis in giant cell arteritis. Ophthalmology. 1993;100(4):550-5.
49. Hayreh SS. Giant cell arteritis: Its ophthalmic manifestations. Indian J Ophthalmol. 2021;69(2):227-35.
50. Gonzalez-Gay MA, Blanco R, Rodriguez-Valverde V, Martinez-Taboada VM, Delgado-Rodriguez M, Figueroa M, et al. Permanent visual loss and cerebrovascular accidents in giant cell arteritis: predictors and response to treatment. Arthritis Rheum. 1998;41(8):1497-504.
51. Hayreh SS, Zimmerman B. Management of giant cell arteritis. Our 27-year clinical study: new light on old controversies. Ophthalmologica. 2003;217(4):239-59.
52. Hayreh SS, Podhajsky PA, Zimmerman B. Occult giant cell arteritis: ocular manifestations. Am J Ophthalmol. 1998;125(4):521-6.
53. Caselli RJ, Hunder GG, Whisnant JP. Neurologic disease in biopsy-proven giant cell (temporal) arteritis. Neurology. 1988;38(3):352-9.
54. Evans JM, O'Fallon WM, Hunder GG. Increased incidence of aortic aneurysm and dissection in giant cell (temporal) arteritis. A population-based study. Ann Intern Med. 1995;122(7):502-7.
55. Mackie SL, Dejaco C, Appenzeller S, Camellino D, Duftner C, Gonzalez-Chiappe S, et al. British Society for Rheumatology guideline on diagnosis and treatment of giant cell arteritis. Rheumatology (Oxford). 2020;59(3):e1-e23.
56. Stone JH, Klearman M, Collinson N. Trial of Tocilizumab in Giant-Cell Arteritis. N Engl J Med. 2017;377(15):1494-5.
57. Turesson C, Borjesson O, Larsson K, Mohammad AJ, Knight A. Swedish Society of Rheumatology 2018 guidelines for investigation, treatment, and follow-up of giant cell arteritis. Scand J Rheumatol. 2019;48(4):259-65.
58. Salvarani C, Hunder GG. Giant cell arteritis with low erythrocyte sedimentation rate: frequency of occurence in a population-based study. Arthritis Rheum. 2001;45(2):140-5.

59. Ellis ME, Ralston S. The ESR in the diagnosis and management of the polymyalgia rheumatica/giant cell arteritis syndrome. Ann Rheum Dis. 1983;42(2):168-70.
60. Weyand CM, Fulbright JW, Hunder GG, Evans JM, Goronzy JJ. Treatment of giant cell arteritis: interleukin-6 as a biologic marker of disease activity. Arthritis Rheum. 2000;43(5):1041-8.
61. Kermani TA, Schmidt J, Crowson CS, Ytterberg SR, Hunder GG, Matteson EL, et al. Utility of erythrocyte sedimentation rate and C-reactive protein for the diagnosis of giant cell arteritis. Semin Arthritis Rheum. 2012;41(6):866-71.
62. Maz M, Chung SA, Abril A, Langford CA, Gorelik M, Guyatt G, et al. 2021 American College of Rheumatology/Vasculitis Foundation Guideline for the Management of Giant Cell Arteritis and Takayasu Arteritis. Arthritis Rheumatol. 2021;73(8):1349-65.
63. Klein RG, Campbell RJ, Hunder GG, Carney JA. Skip lesions in temporal arteritis. Mayo Clin Proc. 1976;51(8):504-10.
64. Poller DN, van Wyk Q, Jeffrey MJ. The importance of skip lesions in temporal arteritis. J Clin Pathol. 2000;53(2):137-9.
65. Oh LJ, Wong E, Gill AJ, McCluskey P, Smith JEH. Value of temporal artery biopsy length in diagnosing giant cell arteritis. ANZ J Surg. 2018;88(3):191-5.
66. Narvaez J, Bernad B, Roig-Vilaseca D, Garcia-Gomez C, Gomez-Vaquero C, Juanola X, et al. Influence of previous corticosteroid therapy on temporal artery biopsy yield in giant cell arteritis. Semin Arthritis Rheum. 2007;37(1):13-9.
67. Dasgupta B, Borg FA, Hassan N, Alexander L, Barraclough K, Bourke B, et al. BSR and BHPR guidelines for the management of giant cell arteritis. Rheumatology (Oxford). 2010;49(8):1594-7.
68. Jakobsson K, Jacobsson L, Mohammad AJ, Nilsson JA, Warrington K, Matteson EL, et al. The effect of clinical features and glucocorticoids on biopsy findings in giant cell arteritis. BMC Musculoskelet Disord. 2016;17(1):363.
69. Font RL, Prabhakaran VC. Histological parameters helpful in recognising steroid-treated temporal arteritis: an analysis of 35 cases. Br J Ophthalmol. 2007;91(2):204-9.
70. Ashton-Key M, Gallagher PJ. Surgical pathology of cranial arteritis and polymyalgia rheumatica. Baillieres Clin Rheumatol. 1991;5(3):387-404.
71. Hernandez-Rodriguez J, Murgia G, Villar I, Campo E, Mackie SL, Chakrabarty A, et al. Description and Validation of Histological Patterns and Proposal of a Dynamic Model of Inflammatory Infiltration in Giant-cell Arteritis. Medicine (Baltimore). 2016;95(8):e2368.
72. Taylor-Gjevre R, Vo M, Shukla D, Resch L. Temporal artery biopsy for giant cell arteritis. J Rheumatol. 2005;32(7):1279-82.
73. Sharma NS, Ooi JL, McGarity BH, Vollmer-Conna U, McCluskey P. The length of superficial temporal artery biopsies. ANZ J Surg. 2007;77(6):437-9.
74. Breuer GS, Nesher R, Nesher G. Effect of biopsy length on the rate of positive temporal artery biopsies. Clin Exp Rheumatol. 2009;27(1 Suppl 52):S10-3.

75. Ypsilantis E, Courtney ED, Chopra N, Karthikesalingam A, Eltayab M, Katsoulas N, et al. Importance of specimen length during temporal artery biopsy. Br J Surg. 2011;98(11):1556-60.
76. Kaptanis S, Perera JK, Halkias C, Caton N, Alarcon L, Vig S. Temporal artery biopsy size does not matter. Vascular. 2014;22(6):406-10.
77. Mahr A, Saba M, Kambouchner M, Polivka M, Baudrimont M, Brocheriou I, et al. Temporal artery biopsy for diagnosing giant cell arteritis: the longer, the better? Ann Rheum Dis. 2006;65(6):826-8.
78. Wong M, Toh L, Wilson A, Rowley K, Karschimkus C, Prior D, et al. Reduced arterial elasticity in rheumatoid arthritis and the relationship to vascular disease risk factors and inflammation. Arthritis Rheum. 2003;48(1):81-9.
79. Booth AD, Wallace S, McEniery CM, Yasmin, Brown J, Jayne DR, et al. Inflammation and arterial stiffness in systemic vasculitis: a model of vascular inflammation. Arthritis Rheum. 2004;50(2):581-8.
80. Su GW, Foroozan R, Yen MT. Quantitative analysis of temporal artery contraction after biopsy for evaluation of giant cell arteritis. Can J Ophthalmol. 2006;41(4):500-3.
81. Gordon LK, Levin LA. Visual loss in giant cell arteritis. JAMA. 1998;280(4):385-6.
82. Gardner ES, Sumner WT, Cook JL. Predictable tissue shrinkage during frozen section histopathologic processing for Mohs micrographic surgery. Dermatol Surg. 2001;27(9):813-8.
83. Blasco-Morente G, Garrido-Colmenero C, Perez-Lopez I, Carretero-Garcia S, Martin-Castro A, Arias-Santiago S, et al. Study of shrinkage of cutaneous surgical specimens. J Cutan Pathol. 2015;42(4):253-7.
84. Danesh-Meyer HV, Savino PJ, Bilyk JR, Eagle RC, Sergott RC. Shrinkage: fact or fiction? Arch Ophthalmol. 2001;119(8):1217.
85. Murchison AP, Bilyk JR, Eagle RC, Jr., Savino PJ. Shrinkage revisited: how long is long enough? Ophthal Plast Reconstr Surg. 2012;28(4):261-3.
86. Thatcher MD, Chan AT, Munoz DG, Micieli JA. Comparison of pre-formalin fixation and postfixation temporal artery biopsy lengths. Can J Ophthalmol. 2023;58(6):539-42.
87. Sudlow C. Diagnosing and managing polymyalgia rheumatica and temporal arteritis. Sensitivity of temporal artery biopsy varies with biopsy length and sectioning strategy. BMJ. 1997;315(7107):549.
88. Hunder GG, Bloch DA, Michel BA, Stevens MB, Arend WP, Calabrese LH, et al. The American College of Rheumatology 1990 criteria for the classification of giant cell arteritis. Arthritis Rheum. 1990;33(8):1122-8.
89. Hunder GG. The use and misuse of classification and diagnostic criteria for complex diseases. Ann Intern Med. 1998;129(5):417-8.
90. Rao JK, Allen NB, Pincus T. Limitations of the 1990 American College of Rheumatology classification criteria in the diagnosis of vasculitis. Ann Intern Med. 1998;129(5):345-52.

91. Duhaut P, Pinede L, Bornet H, Demolombe-Rague S, Dumontet C, Ninet J, et al. Biopsy proven and biopsy negative temporal arteritis: differences in clinical spectrum at the onset of the disease. Groupe de Recherche sur l'Arterite a Cellules Geantes. Ann Rheum Dis. 1999;58(6):335-41.
92. Ing EB, Miller NR, Nguyen A, Su W, Bursztyn L, Poole M, et al. Neural network and logistic regression diagnostic prediction models for giant cell arteritis: development and validation. Clin Ophthalmol. 2019;13:421-30.
93. Gabriel SE, O'Fallon WM, Achkar AA, Lie JT, Hunder GG. The use of clinical characteristics to predict the results of temporal artery biopsy among patients with suspected giant cell arteritis. J Rheumatol. 1995;22(1):93-6.
94. Liozon E, Dalmay F, Lalloue F, Gondran G, Bezanahary H, Fauchais AL, et al. Risk Factors for Permanent Visual Loss in Biopsy-proven Giant Cell Arteritis: A Study of 339 Patients. J Rheumatol. 2016;43(7):1393-9.
95. Cid MC, Font C, Oristrell J, de la Sierra A, Coll-Vinent B, Lopez-Soto A, et al. Association between strong inflammatory response and low risk of developing visual loss and other cranial ischemic complications in giant cell (temporal) arteritis. Arthritis Rheum. 1998;41(1):26-32.
96. Dejaco C, Ramiro S, Bond M, Bosch P, Ponte C, Mackie SL, et al. EULAR recommendations for the use of imaging in large vessel vasculitis in clinical practice: 2023 update. Ann Rheum Dis. 2023.
97. Arida A, Kyprianou M, Kanakis M, Sfikakis PP. The diagnostic value of ultrasonography-derived edema of the temporal artery wall in giant cell arteritis: a second meta-analysis. BMC Musculoskelet Disord. 2010;11:44.
98. Karassa FB, Matsagas MI, Schmidt WA, Ioannidis JP. Meta-analysis: test performance of ultrasonography for giant-cell arteritis. Ann Intern Med. 2005;142(5):359-69.
99. Ball EL, Walsh SR, Tang TY, Gohil R, Clarke JM. Role of ultrasonography in the diagnosis of temporal arteritis. Br J Surg. 2010;97(12):1765-71.
100. Nakajima E, Moon FH, Junior NC, Macedo CR, de Souza AWS, Iared W. Accuracy of Doppler ultrasound in the diagnosis of giant cell arteritis: a systematic review and meta-analysis. Adv Rheumatol. 2023;63(1):5.
101. Rinagel M, Chatelus E, Jousse-Joulin S, Sibilia J, Gottenberg JE, Chasset F, et al. Diagnostic performance of temporal artery ultrasound for the diagnosis of giant cell arteritis: a systematic review and meta-analysis of the literature. Autoimmun Rev. 2019;18(1):56-61.
102. Schmidt WA, Blockmans D. Use of ultrasonography and positron emission tomography in the diagnosis and assessment of large-vessel vasculitis. Curr Opin Rheumatol. 2005;17(1):9-15.
103. Aschwanden M, Kesten F, Stern M, Thalhammer C, Walker UA, Tyndall A, et al. Vascular involvement in patients with giant cell arteritis determined by duplex sonography of 2x11 arterial regions. Ann Rheum Dis. 2010;69(7):1356-9.

104. Schmidt WA, Kraft HE, Vorpahl K, Volker L, Gromnica-Ihle EJ. Color duplex ultrasonography in the diagnosis of temporal arteritis. N Engl J Med. 1997;337(19):1336-42.
105. Chrysidis S, Terslev L, Christensen R, Fredberg U, Larsen K, Lorenzen T, et al. Vascular ultrasound for the diagnosis of giant cell arteritis: a reliability and agreement study based on a standardised training programme. RMD Open. 2020;6(3).
106. Schafer VS, Chrysidis S, Dejaco C, Duftner C, Iagnocco A, Bruyn GA, et al. Assessing Vasculitis in Giant Cell Arteritis by Ultrasound: Results of OMERACT Patient-based Reliability Exercises. J Rheumatol. 2018;45(9):1289-95.
107. Aschwanden M, Daikeler T, Kesten F, Baldi T, Benz D, Tyndall A, et al. Temporal artery compression sign--a novel ultrasound finding for the diagnosis of giant cell arteritis. Ultraschall Med. 2013;34(1):47-50.
108. Diamantopoulos AP, Haugeberg G, Hetland H, Soldal DM, Bie R, Myklebust G. Diagnostic value of color Doppler ultrasonography of temporal arteries and large vessels in giant cell arteritis: a consecutive case series. Arthritis Care Res (Hoboken). 2014;66(1):113-9.
109. Bosch P, Bond M, Dejaco C, Ponte C, Mackie SL, Falzon L, et al. Imaging in diagnosis, monitoring and outcome prediction of large vessel vasculitis: a systematic literature review and meta-analysis informing the 2023 update of the EULAR recommendations. RMD Open. 2023;9(3).
110. Czihal M, Schrottle A, Baustel K, Lottspeich C, Dechant C, Treitl KM, et al. B-mode sonography wall thickness assessment of the temporal and axillary arteries for the diagnosis of giant cell arteritis: a cohort study. Clin Exp Rheumatol. 2017;35 Suppl 103(1):128-33.
111. Aschwanden M, Imfeld S, Staub D, Baldi T, Walker UA, Berger CT, et al. The ultrasound compression sign to diagnose temporal giant cell arteritis shows an excellent interobserver agreement. Clin Exp Rheumatol. 2015;33(2 Suppl 89):S-113-5.
112. Schafer VS, Juche A, Ramiro S, Krause A, Schmidt WA. Ultrasound cut-off values for intima-media thickness of temporal, facial and axillary arteries in giant cell arteritis. Rheumatology (Oxford). 2017;56(9):1632.
113. Pfadenhauer K, Weber H. Duplex sonography of the temporal and occipital artery in the diagnosis of temporal arteritis. A prospective study. J Rheumatol. 2003;30(10):2177-81.
114. Muratore F, Boiardi L, Restuccia G, Macchioni P, Pazzola G, Nicolini A, et al. Comparison between colour duplex sonography findings and different histological patterns of temporal artery. Rheumatology (Oxford). 2013;52(12):2268-74.
115. Restuccia G, Cavazza A, Boiardi L, Pipitone N, Macchioni P, Bajocchi G, et al. Small-vessel vasculitis surrounding an uninflamed temporal artery and isolated vasa vasorum vasculitis of the temporal artery: two subsets of giant cell arteritis. Arthritis Rheum. 2012;64(2):549-56.

116. Hauenstein C, Reinhard M, Geiger J, Markl M, Hetzel A, Treszl A, et al. Effects of early corticosteroid treatment on magnetic resonance imaging and ultrasonography findings in giant cell arteritis. Rheumatology (Oxford). 2012;51(11):1999-2003.
117. Ponte C, Serafim AS, Monti S, Fernandes E, Lee E, Singh S, et al. Early variation of ultrasound halo sign with treatment and relation with clinical features in patients with giant cell arteritis. Rheumatology (Oxford). 2020;59(12):3717-26.
118. Bley TA, Reinhard M, Hauenstein C, Markl M, Warnatz K, Hetzel A, et al. Comparison of duplex sonography and high-resolution magnetic resonance imaging in the diagnosis of giant cell (temporal) arteritis. Arthritis Rheum. 2008;58(8):2574-8.
119. Narvaez J, Narvaez JA, Nolla JM, Sirvent E, Reina D, Valverde J. Giant cell arteritis and polymyalgia rheumatica: usefulness of vascular magnetic resonance imaging studies in the diagnosis of aortitis. Rheumatology (Oxford). 2005;44(4):479-83.
120. Vaidyanathan S, Chattopadhyay A, Mackie SL, Scarsbrook AF. Comparative effectiveness of (18)F-FDG PET-CT and contrast-enhanced CT in the diagnosis of suspected large-vessel vasculitis. Br J Radiol. 2018;91(1089):20180247.
121. Hall JK. Giant-cell arteritis. Curr Opin Ophthalmol. 2008;19(6):454-60.
122. Dejaco C, Ramiro S, Duftner C, Besson FL, Bley TA, Blockmans D, et al. EULAR recommendations for the use of imaging in large vessel vasculitis in clinical practice. Ann Rheum Dis. 2018;77(5):636-43.
123. Prieto-Gonzalez S, Arguis P, Garcia-Martinez A, Espigol-Frigole G, Tavera-Bahillo I, Butjosa M, et al. Large vessel involvement in biopsy-proven giant cell arteritis: prospective study in 40 newly diagnosed patients using CT angiography. Ann Rheum Dis. 2012;71(7):1170-6.
124. Ntziachristos V, Razansky D. Molecular imaging by means of multispectral optoacoustic tomography (MSOT). Chem Rev. 2010;110(5):2783-94.
125. Yao J, Wang LV. Photoacoustic tomography: fundamentals, advances and prospects. Contrast Media Mol Imaging. 2011;6(5):332-45.
126. Attia ABE, Balasundaram G, Moothanchery M, Dinish US, Bi R, Ntziachristos V, et al. A review of clinical photoacoustic imaging: Current and future trends. Photoacoustics. 2019;16:100144.
127. Jeon S, Song HB, Kim J, Lee BJ, Managuli R, Kim JH, et al. In Vivo Photoacoustic Imaging of Anterior Ocular Vasculature: A Random Sample Consensus Approach. Sci Rep. 2017;7(1):4318.
128. Zafar H, Breathnach A, Subhash HM, Leahy MJ. Linear-array-based photoacoustic imaging of human microcirculation with a range of high frequency transducer probes. J Biomed Opt. 2015;20(5):051021.
129. Xu D, Yang S, Wang Y, Gu Y, Xing D. Noninvasive and high-resolving photoacoustic dermoscopy of human skin. Biomed Opt Express. 2016;7(6):2095-102.

130. Daeichin V, Wu M, De Jong N, van der Steen AF, van Soest G. Frequency Analysis of the Photoacoustic Signal Generated by Coronary Atherosclerotic Plaque. Ultrasound Med Biol. 2016;42(8):2017-25.
131. Kruizinga P, van der Steen AF, de Jong N, Springeling G, Robertus JL, van der Lugt A, et al. Photoacoustic imaging of carotid artery atherosclerosis. J Biomed Opt. 2014;19(11):110504.
132. Karlas A, Reber J, Diot G, Bozhko D, Anastasopoulou M, Ibrahim T, et al. Flow-mediated dilatation test using optoacoustic imaging: a proof-of-concept. Biomed Opt Express. 2017;8(7):3395-403.
133. Taruttis A, Timmermans AC, Wouters PC, Kacprowicz M, van Dam GM, Ntziachristos V. Optoacoustic Imaging of Human Vasculature: Feasibility by Using a Handheld Probe. Radiology. 2016;281(1):256-63.
134. Merdasa A, Bunke J, Naumovska M, Albinsson J, Erlov T, Cinthio M, et al. Photoacoustic imaging of the spatial distribution of oxygen saturation in an ischemia-reperfusion model in humans. Biomed Opt Express. 2021;12(4):2484-95.
135. Matsumoto Y, Asao Y, Yoshikawa A, Sekiguchi H, Takada M, Furu M, et al. Label-free photoacoustic imaging of human palmar vessels: a structural morphological analysis. Sci Rep. 2018;8(1):786.
136. Sheikh R, Cinthio M, Dahlstrand U, Erlov T, Naumovska M, Hammar B, et al. Clinical Translation of a Novel Photoacoustic Imaging System for Examining the Temporal Artery. IEEE Trans Ultrason Ferroelectr Freq Control. 2019;66(3):472-80.
137. Erlov T, Cinthio M, Edsfeldt A, Segstedt S, Dias N, Nilsson J, et al. Determining carotid plaque vulnerability using ultrasound center frequency shifts. Atherosclerosis. 2016;246:293-300.
138. Rogers S, Carreira J, Thompson R, Morais A, Miller C, Wein W, et al. An Ex Vivo Evaluation of Tomographic 3-D Ultrasound, B-Mode Ultrasound, CT And MR Imaging to Measure Artery Diameter, Length and Wall Volume. Ultrasound Med Biol. 2019;45(10):2819-29.
139. Alzahrani A, Sultan SR, Aslam M. Tomographic 3D ultrasound for grading stenosis of superficial femoral artery. Perfusion. 2023:2676591231169852.
140. Ball S, Rogers S, Kanesalingam K, Taylor R, Katsogridakis E, McCollum C. Carotid plaque volume in patients undergoing carotid endarterectomy. Br J Surg. 2018;105(3):262-9.
141. Khan M, Rogers S, Carreira J, Ghosh J, McCollum C. Aneurysm Geometry Analyzed by the Novel Three-Dimensional Tomographic Ultrasound Relates to Abdominal Aortic Aneurysm Growth. Ann Vasc Surg. 2022;87:469-77.
142. Steinberg I, Huland DM, Vermesh O, Frostig HE, Tummers WS, Gambhir SS. Photoacoustic clinical imaging. Photoacoustics. 2019;14:77-98.
143. Wu D, Huang L, Jiang MS, Jiang H. Contrast agents for photoacoustic and thermoacoustic imaging: a review. Int J Mol Sci. 2014;15(12):23616-39.
144. IEC. Safety of laser products – Part 1: Equipment classification and requirements. International Standard IEC 60825-12014.

145. FDA. Information for Manufacturers Seeking Marketing Clearance of Diagnostic Ultrasound Systems and Transducers. In: Services USDoHaH, editor. Guidance for Industry and FDA Staff: Food and Drug Administration; 2008.
146. BMUS. Guidelines for the safe use of diagnostic ultrasound equipment. The British Medical Ultrasound Society; 2010.
147. Frisen L, Kalm H. Sahlgren's saturation test for detecting and grading acquired dyschromatopsia. Am J Ophthalmol. 1981;92(2):252-8.
148. Hult J, Merdasa A, Pekar-Lukacs A, Tordengren Stridh M, Khodaverdi A, Albinsson J, et al. Comparison of photoacoustic imaging and histopathological examination in determining the dimensions of 52 human melanomas and nevi ex vivo. Biomed Opt Express. 2021;12(7):4097-114.
149. Erlov T, Jansson T, Persson HW, Cinthio M. Scatterer size estimation using the center frequency assessed from ultrasound time domain data. J Acoust Soc Am. 2016;140(4):2352.
150. Zafar H, Breathnach A, Subhash HM, Leahy MJ. Linear-array-based photoacoustic imaging of human microcirculation with a range of high frequency transducer probes. J Biomed Opt. 2015;20(5):051021.
151. Bok T-H, Hysi E, Kolios MC. Preliminary photoacoustic imaging of the human radial artery for simultaneous assessment of red blood cell aggregation and oxygen saturation in vivo. Proc 2017 IEEE International Ultrasonics Symposium 2017.
152. Hai P, Zhou Y, Liang J, Li C, Wang LV. Photoacoustic tomography of vascular compliance in humans. J Biomed Opt. 2015;20(12):126008.
153. Maldini C, Depinay-Dhellemmes C, Tra TT, Chauveau M, Allanore Y, Gossec L, et al. Limited value of temporal artery ultrasonography examinations for diagnosis of giant cell arteritis: analysis of 77 subjects. J Rheumatol. 2010;37(11):2326-30.
154. Salvarani C, Silingardi M, Ghirarduzzi A, Lo Scocco G, Macchioni P, Bajocchi G, et al. Is duplex ultrasonography useful for the diagnosis of giant-cell arteritis? Ann Intern Med. 2002;137(4):232-8.
155. Rogers SK, Phair A, Carriera J, Ghosh J, Bowling FL, McCollum C. Feasibility and Accuracy of Measuring Carotid Plaque Volume (Burden) With Contrast-Enhanced Tomographic 3D Ultrasound and Ultrasound Image Fusion. Ann Vasc Surg. 2023;91:168-75.
156. Hughes M, Rogers S, Carreira J, Moore T, Manning J, Dinsdale G, et al. Imaging digital arteries in systemic sclerosis by tomographic 3-dimensional ultrasound. Rheumatol Int. 2021;41(6):1089-96.
157. Cox B, Laufer JG, Arridge SR, Beard PC. Quantitative spectroscopic photoacoustic imaging: a review. J Biomed Opt. 2012;17(6):061202.
158. Bulsink R, Kuniyil Ajith Singh M, Xavierselvan M, Mallidi S, Steenbergen W, Francis KJ. Oxygen Saturation Imaging Using LED-Based Photoacoustic System. Sensors (Basel). 2021;21(1).

159. Tzoumas S, Nunes A, Olefir I, Stangl S, Symvoulidis P, Glasl S, et al. Eigenspectra optoacoustic tomography achieves quantitative blood oxygenation imaging deep in tissues. Nat Commun. 2016;7:12121.
160. Erlov T, Sheikh R, Dahlstrand U, Albinsson J, Malmsjo M, Cinthio M. Regional motion correction for in vivo photoacoustic imaging in humans using interleaved ultrasound images. Biomed Opt Express. 2021;12(6):3312-22.